

2-Arylpirazolo[4,3-*d*]pyrimidin-7-amino Derivatives As New Potent and Selective Human A₃ Adenosine Receptor Antagonists. Molecular Modeling Studies and Pharmacological Evaluation

Lucia Squarcialupi,[†] Vittoria Colotta,^{*,†} Daniela Catarzi,[†] Flavia Varano,[†] Guido Filacchioni,[†] Katia Varani,[‡] Carmen Corciulo,[‡] Fabrizio Vincenzi,[‡] Pier Andrea Borea,[‡] Carla Ghelardini,[§] Lorenzo Di Cesare Mannelli,[§] Antonella Ciancetta,[#] and Stefano Moro^{*,#}

[†]Dipartimento di Neuroscienze, Psicologia, Area del Farmaco e Salute del Bambino, Sezione di Farmaceutica e Nutraceutica, Università di Firenze, Via Ugo Schiff, 6, 50019 Sesto Fiorentino, Italy

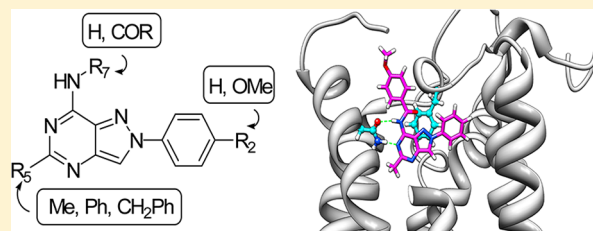
[‡]Dipartimento di Scienze Mediche, Istituto di Farmacologia, Università di Ferrara, Via Fossato di Mortara 17-19, 44121 Ferrara, Italy

[§]Dipartimento di Neuroscienze, Psicologia, Area del Farmaco e Salute del Bambino, Sezione di Farmacologia e Tossicologia, Viale Pieraccini, 6, 50139 Firenze, Italy

[#]Molecular Modeling Section (MMS), Dipartimento di Scienze del Farmaco, Università di Padova, via Marzolo 5, 35131 Padova, Italy

Supporting Information

ABSTRACT: On the basis of our previously reported 2-arylpirazolo[4,3-*d*]pyrimidin-7-ones, a set of 2-arylpirazolo[4,3-*d*]pyrimidin-7-amines were designed as new human (h) A₃ adenosine receptor (AR) antagonists. Lipophilic groups with different steric bulk were introduced at the 5-position of the bicyclic scaffold (R₅ = Me, Ph, CH₂Ph), and different acyl and carbamoyl moieties (R₇) were appended on the 7-amino group, as well as a para-methoxy group inserted on the 2-phenyl ring. The presence of acyl groups turned out to be of paramount importance for an efficient and selective binding at the hA₃ AR. In fact, most of the 7-acylamino derivatives showed low nanomolar affinity (K_i = 2.5–45 nM) and high selectivity toward this receptor. A few selected pyrazolo[4,3-*d*]pyrimidin-7-amides were effective in counteracting oxaliplatin-induced apoptosis in rat astrocyte cell cultures, an *in vitro* model of neurotoxicity. Through an *in silico* receptor-driven approach the obtained binding data were rationalized and the molecular bases of the observed hA₃ AR affinity and hA₃ versus hA_{2A} AR selectivity were explained.



INTRODUCTION

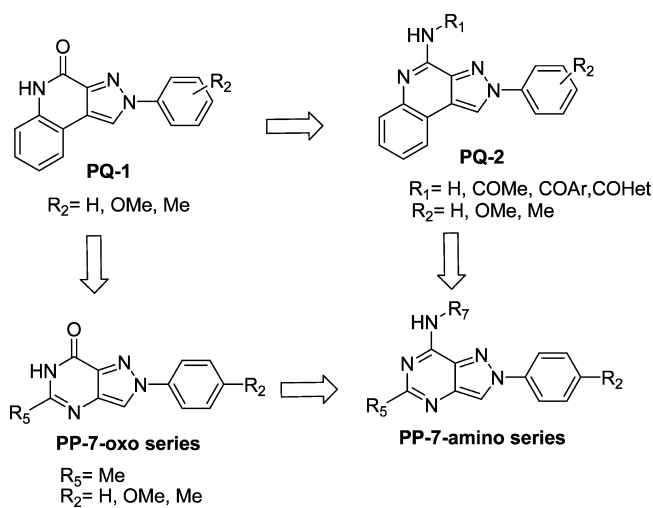
Adenosine is a ubiquitous purine nucleoside that acts as a modulator of many cell functions, both in normal and pathological conditions. The wide variety of effects exerted by adenosine is due to activation of four G-protein-coupled receptors (GPCRs), classified as A₁, A_{2A}, A_{2B}, and A₃ subtypes.^{1–3} Adenosine receptors (ARs) are coupled to adenylyl cyclase that can be both inhibited (A₁ and A₃) or activated (A_{2A} and A_{2B}).¹ Moreover, ARs are also associated to other second messenger signaling pathways. In particular, the A₃ AR activates phospholipase C,⁴ causing an increase of intracellular calcium levels, and modulates protein kinase C activity⁴ as well as K_{ATP} channel.⁵ The A₃ AR also controls the activity of mitogen-activated protein kinases (MAPK), such as the extracellular signal-regulated kinase (ERK) 1/2 and the stress-activated protein kinase p38.⁶ These latter effects account for the role of adenosine in the regulation of cell proliferation and differentiation, although the understanding of the A₃-signaling in these processes is far from being completely clarified. In humans, the A₃ AR was found in many peripheral tissues such as lung, liver, and immune cells, and it is

overexpressed in different tumor cell types.⁷ The A₃ AR regulation of the cell cycle may induce both cell protection or cell death, depending on the degree of receptor activation and/or the cell type or toxic insult.^{6–9} Thus, both A₃ receptor agonists and antagonists might be effective agents in cancer therapy.^{7–9} In the central nervous system (CNS), the A₃ AR is expressed both in neurons and glial cells, such as microglia and astrocytes, which are recognized both as structural support for neurons and as active participants in various pathological conditions, as neurodegenerative diseases, trauma, and neuropathic pain.^{10–12} Also in the CNS, activation of the A₃ AR may afford both pro- and antisurvival effects, thus inducing either protection or damage, depending on the situation.^{6,8,13} Hence, even though it has been clearly demonstrated that the A₃ AR is involved in many disease pathways, much research is needed to understand in depth the roles played by this receptor. Therefore, the search for new selective A₃ AR ligands, either agonists or antagonists, still remains an attractive objective.¹⁴

Received: September 24, 2012

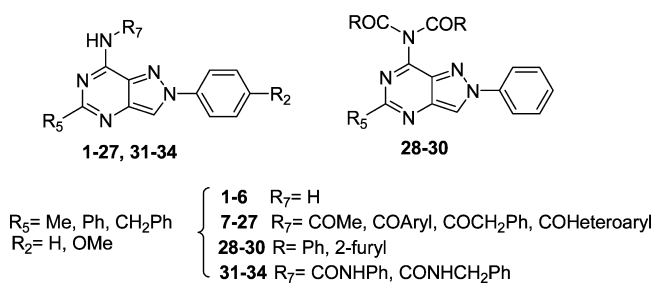
In our laboratory we have devoted much research to the study of AR antagonists belonging to different heterocyclic classes. Within the investigated series, many potent and selective antagonists for the A₃ receptor subtype were identified.^{15–26} Most of them are tricyclic derivatives, thus highly lipophilic and with low water solubility, and this often makes it difficult to test them in pharmacological assays. To overcome this drawback, our recent studies have been directed to the identification of new bicyclic scaffolds^{21,25,26} to obtain more soluble AR antagonists. This strategy afforded diverse classes of compounds, such as the recently investigated pyrazolo[4,3-*d*]pyrimidin-7-one derivatives²⁵ (PP-7-oxo series), designed as analogues of previously reported pyrazolo[3,4-*c*]quinolin-4-ones (PQ-1 series, Chart 1). Most of the PP-7-oxo

Chart 1. Structural Modification Approach from the Pyrazolo[3,4-*c*]quinoline Series to the Pyrazolo[4,3-*d*]pyrimidine Derivatives



compounds were highly potent and selective hA₃ antagonists, thus indicating that the pyrazolo[4,3-*d*]pyrimidine ring system can be considered as a good scaffold for the development of hA₃ AR antagonists. Hence, we decided to replace the 7-oxo function of the PP series with an amino group (PP-7-amino series, Chart 1), as it was performed on the previously reported PQ-1 series to give the corresponding 4-amines (PQ-2 series, Chart 1) which turned out potent AR antagonists.^{16,20,23,27} The herein reported 2-arylpyrazolo[4,3-*d*]pyrimidin-7-amino derivatives 1–34 (Chart 2) bear substituents with different lipophilicity and steric bulk at the 5-position ($R_5 = \text{Me, Ph, CH}_2\text{Ph}$). Moreover, a 4-methoxy group (R_2) was inserted on

Chart 2. Herein Reported 2-Arylpyrazolo[4,3-*d*]pyrimidin-7-amino Derivatives 1–34

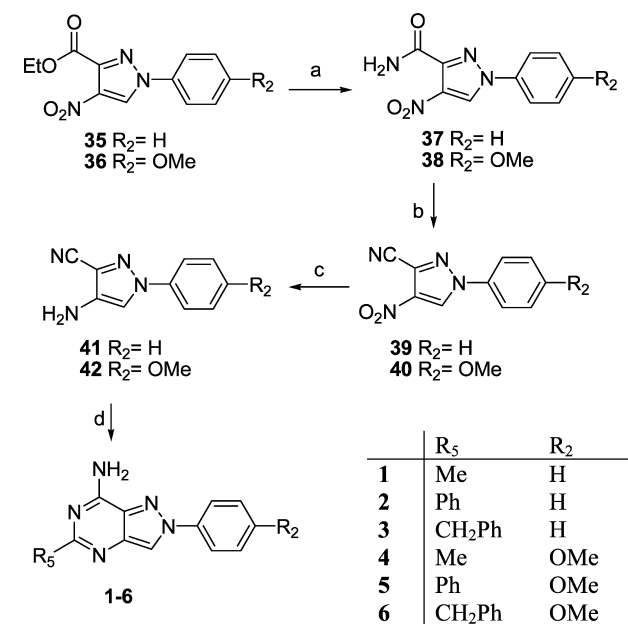


the 2-phenyl ring, and acyl residues ($R_7 = \text{COMe, COAr, COCH}_2\text{Ph, COHeteroaryl}$) or carbamoyl moieties ($R_7 = \text{CONHPh, CONHCH}_2\text{Ph}$) were placed on the 7-amino group. The choice of these R_7 and R_2 substituents was made since they increased hA₃AR affinity and selectivity both in our previously described derivatives^{15–24} and in many other classes of AR antagonists of similar size and shape.¹⁴ Molecular modeling studies were carried out to explain both hA₃ affinity and selectivity profiles of the new antagonists. Since A₃AR modulation was described as relevant in chemotherapy-induced neuropathy,¹² some selected pyrazolo[4,3-*d*]pyrimidines (compounds 8, 17, 26, 27), showing high hA₃ AR affinity and selectivity, were evaluated in a rat cellular model of chemotherapy-induced neurotoxicity.

CHEMISTRY

The synthesis of the pyrazolo[4,3-*d*]pyrimidin-7-amines 1–6 (Scheme 1) started from the ethyl 1-aryl-4-nitropyrazole-3-

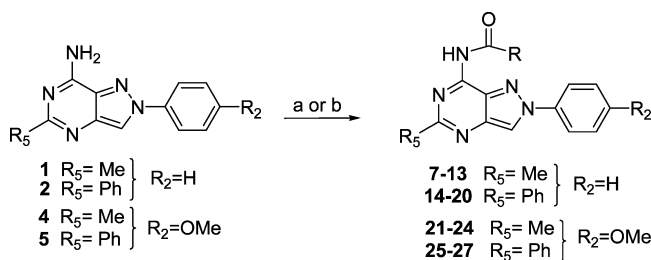
Scheme 1^a



^aReagents and conditions: (a) 33% aqueous NH₃; (b) POCl₃, mw, 120 or 160 °C; (c) cyclohexene, Pd/C, mw, 150 °C; (d) CH₃-C(OEt)₃ or Ph-C(OEt)₃ or PhCH₂-C(=NH)OEt hydrochloride, NH₄OAc, mw, 110 °C.

carboxylates 35 and 36,²⁵ which were treated with 33% aqueous solution of ammonia to yield the 4-nitro-1-aryl-3-carboxamides 37 and 38.²⁵ These compounds were reacted with phosphorus oxychloride under microwave irradiation to give the 4-nitro-1-aryl-3-carbonitriles 39 and 40. Permitting compounds 39 and 40 to react with cyclohexene and Pd/C, under microwave irradiation, the 4-amino derivatives 41 and 42 were obtained. These compounds were transformed into the 5-substituted pyrazolopyrimidin-7-amines 1–6 by a one-pot, three-component, solvent-free reaction with the commercially available triethyl orthoacetate (compounds 1 and 4) or triethyl orthobenzoate (compounds 2 and 5), and ammonium acetate under microwave irradiation. Since triethyl orthophenylacetate was not commercial, the ethyl phenyliminoacetate²⁸ was employed to introduce the benzyl group at the 5-position (compounds 3 and 6). The 7-acylamines 7–27 were prepared

by using two different reaction conditions (Scheme 2). Derivatives **7**, **9**, **11**, **14**, **16–18**, **21**, and **24–27** were obtained

Scheme 2^a

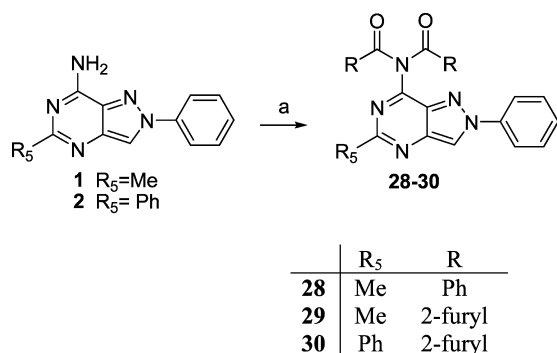
	R
7, 14, 21, 25	Me
8, 15, 22, 26	C ₆ H ₅
9, 16	C ₆ H ₄ -4-OMe
10, 17, 23, 27	CH ₂ C ₆ H ₅
11, 18, 24	2-furyl
12, 19	3-pyridyl
13, 20	4-pyridyl

^aReagent and conditions: (a) RCOCl, anhydrous pyridine, anhydrous methylene chloride, room temperature or reflux; (b) suitable carboxylic acid, 1-hydroxybenzotriazole, NEt₃, 4-(dimethylamino)pyridine, 1-(3-(dimethylamino)propyl)-3-ethylcarbodiimide hydrochloride, DMF, room temperature.

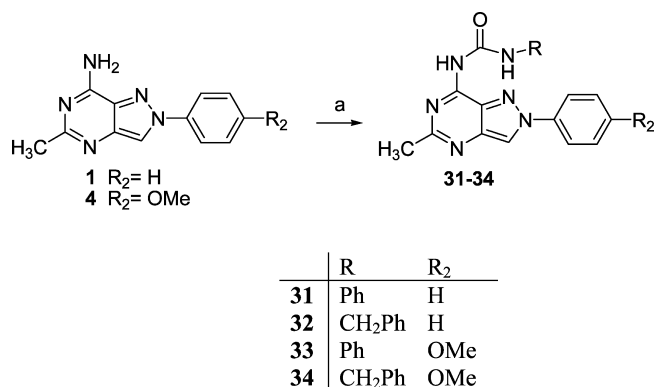
by reacting the pyrazolopyrimidin-7-amines **1**, **2**, **4**, and **5** with the suitable acyl chloride in anhydrous methylene chloride and pyridine. Instead, compounds **8**, **10**, **12**, **13**, **15**, **19**, **20**, **22**, and **23** were synthesized by reacting the 7-amines **1**, **2**, and **4** with the suitable carboxylic acid in dimethylformamide and in the presence of 1-(3-(dimethylamino)propyl)-3-ethylcarbodiimide hydrochloride, 1-hydroxybenzotriazole, triethylamine, and 4-(dimethylamino)pyridine. When compounds **1** and **2** were treated with an excess of benzoyl- and 2-furoyl-chloride, in anhydrous methylene chloride and pyridine, the corresponding 7-diacylamino-substituted derivatives **28–30** were obtained (Scheme 3). Finally, the synthesis of the 7-ureido derivatives **31–34** was achieved by refluxing compounds **1**, **4**, and the suitable isocyanate in anhydrous tetrahydrofuran (Scheme 4).

PHARMACOLOGICAL ASSAYS

The synthesized derivatives **1–34** were tested to evaluate their affinity at hA₁, hA_{2A}, and hA₃ ARs. Compounds were also tested

Scheme 3^a

^aReagents and conditions: (a) RCOCl, anhydrous pyridine, methylene chloride, room temperature or reflux.

Scheme 4^a

^aReagents and conditions: (a) R-NCO, anhydrous tetrahydrofuran, reflux.

at the hA_{2B} AR subtype by measuring their inhibitory effects on NECA-stimulated cAMP levels in CHO cells stably transfected with the hA_{2B} AR. Finally, the antagonistic potency of some selected pyrazolopyrimidin-7-amino derivatives (**8**, **14**, **15**, **17**, **22**, **26–28**) was assessed by evaluating their effect on Cl-IB-MECA-inhibited cAMP production in CHO cells, stably expressing hA₃ ARs. All pharmacological data are collected in Table 1. The selected pyrazolopyrimidine derivatives **8**, **17**, **26–27** were tested to evaluate their effect in counteracting oxaliplatin-induced apoptosis in rat astrocyte cell cultures, an in vitro model of neurotoxicity. As a consequence of this study, these compounds were evaluated for their affinity at the rat A₃ AR, stably expressed in HEK cells. The rat A₃ binding data are included in Table 1.

MOLECULAR MODELING

To rationalize the structure-affinity relationships (SARs) and the selectivity profiles of the new pyrazolopyrimidin-7-amino derivatives, a receptor-driven molecular modeling investigation was carried out. With the aim to identify the hypothetical binding modes of the new compounds, docking simulations inside the binding cavity of the hA₃ AR receptor subtype were performed. As, to date, no crystallographic information about the A₃ AR is available, we used a previously reported hA₃ AR homology model,²⁵ which was built by using the crystal structure of the hA_{2A} AR²⁹ as a template. Moreover, docking simulations at the hA_{2A} AR binding site were also carried out to explain the observed hA_{2A}/hA₃ AR selectivity profiles.

Furthermore, to analyze the ligand-receptor recognition mechanism in a more quantitative fashion, the individual electrostatic and hydrophobic contributions to the interaction energy of each receptor residue involved in the binding with the ligands were also calculated for selected binding poses. The analysis of these contributions afforded “interaction energy fingerprints” (IEFs), i.e., interaction energy patterns, graphically displayed as histograms, reporting the key residues involved in the binding with the considered ligands along with a quantitative estimate of the occurring interactions. This analysis has provided clues on the underlying recognition mechanism that might occur between the new derivatives and the considered receptor subtypes. Moreover, the semiquantitative estimate of the interactions has allowed a direct comparison of different ligands with respect to the quality of ligand-receptor contacts.

Table 1. Binding Affinity (K_i) at hA_1 , hA_{2A} , and hA_3 ARs and Potencies (IC_{50}) at hA_{2B} and hA_3 ARs

	R_5	R_2	R_7	binding experiments ^a K_i (nM) or I%				cAMP assays IC_{50} (nM) or I%	
				hA_1 ^b	hA_{2A} ^c	hA_3 ^d	rA_3 ^e	hA_{2B} ^f	hA_3 ^g
A	Me	H		1%	1%	16 ± 2		2%	
B	Ph	H		22%	10%	10%		4%	
C	CH ₂ Ph	H		11%	1%	900 ± 95		4%	
1	Me	H	H	70 ± 6	246 ± 23	40%		320 ± 35	
2	Ph	H	H	75 ± 7	325 ± 34	48%		440 ± 43	
3	Ph-CH ₂	H	H	150 ± 12	110 ± 10	39%		420 ± 38	
4	Me	4-OMe	H	30%	1%	38%		2%	
5	Ph	4-OMe	H	12%	35%	75 ± 8		3%	
6	Ph-CH ₂	4-OMe	H	40%	37%	45%		33%	
7	Me	H	COMe	25%	4%	300 ± 26		5%	
8	Me	H	COPh	30%	1%	5.6 ± 0.5	6%	2%	19.7 ± 1.8
9	Me	H	CO-C ₄ H ₄ -4-OMe	4%	1%	2.4 ± 0.2		1%	
10	Me	H	COCH ₂ Ph	510 ± 47	13%	120 ± 11		1%	
11	Me	H	CO-2-furyl	20%	1%	20 ± 2		1%	
12	Me	H	CO-3-pyridyl	12%	1%	5.3 ± 0.5		1%	
13	Me	H	CO-4-pyridyl	12%	1%	5.2 ± 0.5		1%	
14	Ph	H	COMe	5%	5%	32 ± 3		2%	103 ± 10
15	Ph	H	COPh	5%	5%	20 ± 2		2%	65 ± 6
16	Ph	H	CO-C ₄ H ₄ -4-OMe	3%	1%	7.3 ± 0.7		1%	
17	Ph	H	COCH ₂ Ph	5%	5%	18 ± 2	2%	2%	61 ± 5
18	Ph	H	CO-2-furyl	11%	1%	24 ± 2.3		1%	
19	Ph	H	CO-3-pyridyl	1%	1%	3.2 ± 0.3		1%	
20	Ph	H	CO-4-pyridyl	1%	1%	25 ± 2		1%	
21	Me	4-OMe	COMe	30%	30%	100 ± 11		30%	
22	Me	4-OMe	COPh	1%	7%	35 ± 4		1%	128 ± 11
23	Me	4-OMe	COCH ₂ Ph	9%	11%	520 ± 52		11%	
24	Me	4-OMe	CO-2-furyl	6%	6%	45 ± 4		1%	
25	Ph	4-OMe	COMe	1%	11%	98 ± 10		1%	
26	Ph	4-OMe	COPh	3%	1%	18 ± 2	12%	2%	63 ± 5
27	Ph	4-OMe	COCH ₂ Ph	29%	18%	24 ± 3	3%	2%	80 ± 9
28	Me		COPh	6%	1%	33 ± 4		5%	115 ± 12
29	Me		CO-2-furyl	4%	1%	33 ± 3		1%	
30	Ph		CO-2-furyl	3%	1%	75 ± 6		1%	
31	Me	H	CONHPh	1%	1%	30%		1%	
32	Me	H	CONHCH ₂ Ph	26%	7%	1%		10%	
33	Me	4-OMe	CONHPh	5%	13%	1%		13%	
34	Me	4-OMe	CONHCH ₂ Ph	8%	7%	6%		1%	

^a K_i values are means ± SEM of four separate assays each performed in duplicate. Percentage of inhibition (I%) is determined at 1 μ M concentration of the tested compounds. ^bDisplacement of specific [³H]DPCPX competition binding assays to hA_1 CHO cells. ^cDisplacement of specific [³H]ZM241385 competition binding to hA_{2A} CHO cells. ^dDisplacement of specific [¹²⁵I]AB-MECA competition binding to hA_3 CHO cells. ^ePercentage of inhibition (I%) in [¹²⁵I]AB-MECA competition binding assays to rA_3 HEK cells. ^fcAMP experiments in hA_{2B} CHO cells, stimulated by 200 nM NECA. IC_{50} values are expressed as means ± SEM of four separate cAMP experiments. Percentage of inhibition (I%) is determined at 1 μ M concentration of the tested compounds. ^g IC_{50} values are expressed as means ± SEM of four separate cAMP experiments in hA_3 CHO cells, in the presence of 100 nM Cl-IB-MECA.

A more detailed description of all the methods used to perform the receptor-driven molecular modeling investigation is reported in the Experimental Section.

RESULTS AND DISCUSSION

Structure-Affinity Relationship Studies. The affinity data of the newly synthesized pyrazolo[4,3-*d*]pyrimidin-7-amino derivatives 1–34 at ARs are reported in Table 1, together with those of the pyrazolo[4,3-*d*]pyrimidin-7-ones A–

C, included as reference compounds. The obtained results indicate that we achieved our goal because most of the 7-acylamino-substituted derivatives 7–30, designed to target the hA_3 receptor, are endowed with nanomolar affinity and high selectivity toward this receptor subtype, the best being the 7-(4-methoxybenzoylamino)-5-methyl-2-phenyl-substituted derivative 9 ($K_i = 2.4$ nM).

Analyzing the binding results, we can observe that replacement of the 7-oxo group (derivatives A–C) with the

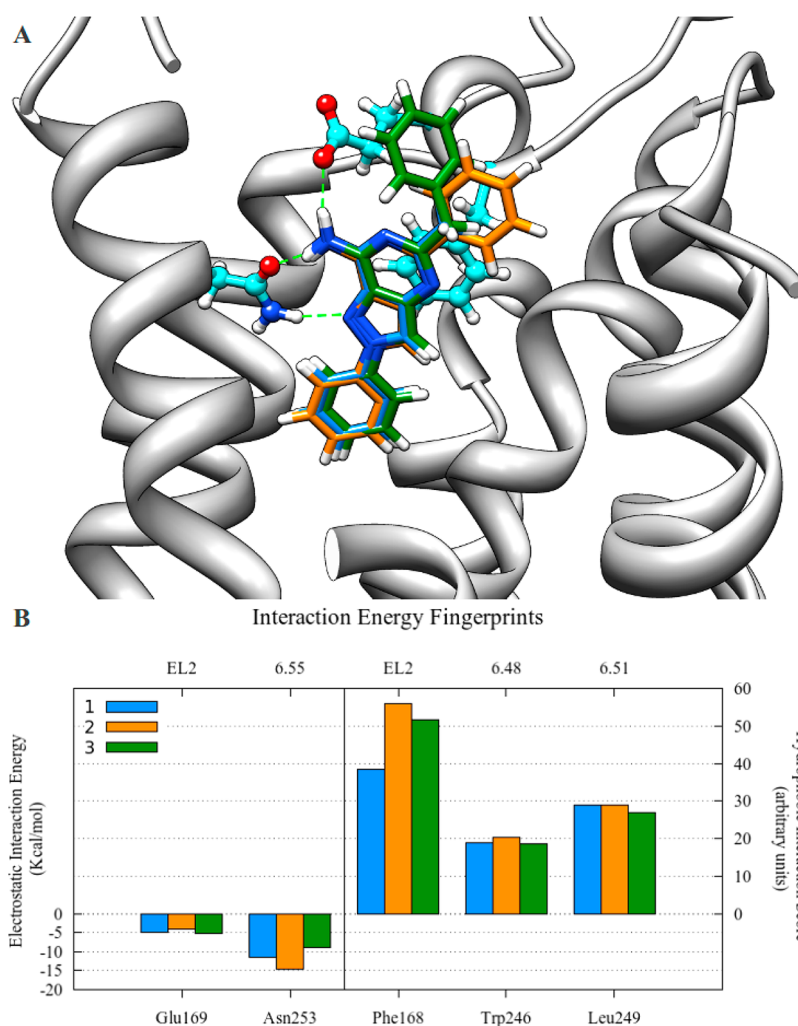


Figure 1. (A) Superimposition of the most energetically favored docking poses of compound **1**, **2** and **3** inside the hA_{2A} AR binding site. The poses are viewed from the membrane side facing TM6, TM7, and TM1. To aid visualization, the view of TM7 is partially omitted and hydrogen atoms are not displayed. Side chains of some amino acids important for ligand recognition and hydrogen bond interactions are highlighted. (B) Interaction energy fingerprints (IEFs) computed for the most energetically favored docking poses of compounds **1**, **2**, and **3**; electrostatic interaction energy values and hydrophobic interaction scores are expressed in kcal/mol and arbitrary hydrophobic units, respectively.

7-amino (compounds **1–3**) significantly modified AR affinity and selectivity. Indeed, while the 7-oxo substituted compounds **A**, **C** are hA₃ AR selective antagonists, and **B** is devoid of affinity for all the ARs, the corresponding 7-amino derivatives **1–3** show good affinity for hA₁, hA_{2A}, and hA_{2B} ARs, and low binding activity at the hA₃ receptor (*I*% = 39–48 at 1 μM). To increase affinity for this last subtype a para methoxy group was introduced on the 2-phenyl ring of derivatives **1–3** to give compounds **4–6**. This modification was undertaken because in several AR antagonists belonging to our series it was one of the most advantageous for improving hA₃ AR affinity and selectivity.^{15–24} Contrary to our expectations, it did not always induce a profitable effect in the herein reported compounds. Indeed, among 2-(4-methoxyphenyl)-substituted derivatives **4–6**, only compound **5** (R₅ = Ph) possesses nanomolar hA₃ AR affinity and high selectivity, while both derivatives **4** (R₅ = Me) and **6** (R₅ = CH₂Ph) maintain the low hA₃ affinity of the parent 2-phenyl-substituted **1** and **3**, and they are also scarcely active at the other ARs. Notable results were obtained when acyl groups were appended on the 7-amino function of the 2-phenyl derivatives **1** (R₅ = Me) and **2** (R₅ = Ph), to give compounds **7–13** and **14–20**, respectively. This structural modification

completely shifted affinity toward the hA₃ receptor. In fact, all the 7-amido-substituted pyrazolopyrimidines showed nanomolar affinities for the hA₃ AR and almost null activities at the other AR subtypes, the only exception being the 5-methyl-7-phenylacetamido derivative **10** which was endowed with a certain hA₁ AR binding affinity (*K*_i = 510 nM). The acetamino-substituted derivatives **7** and **14** demonstrated, respectively, good (*K*_i = 300 nM) and high (*K*_i = 32 nM) affinity for the hA₃ receptor. Replacement of the small acetyl group with the bulkier and more lipophilic benzoyl moiety (derivatives **8** and **15**) increased the capability to bind the hA₃ receptor, in particular for compound **8**, which is about 50-fold more active than the corresponding 7-acetamido derivative **7**. When the benzoyl group was replaced with the phenylacetyl moiety, the A₃ AR affinity was 20-fold reduced (compound **10**) or unchanged (compound **17**).

Because the 7-benzoylamino-substituted derivatives **8** and **15** showed the higher hA₃ affinity and selectivity they were taken as leads to be optimized. Thus, a para-methoxy substituent was introduced on the benzoyl group to afford compounds **9** and **16**, respectively. This modification caused a further enhancement of the hA₃ receptor binding and led to the best antagonist

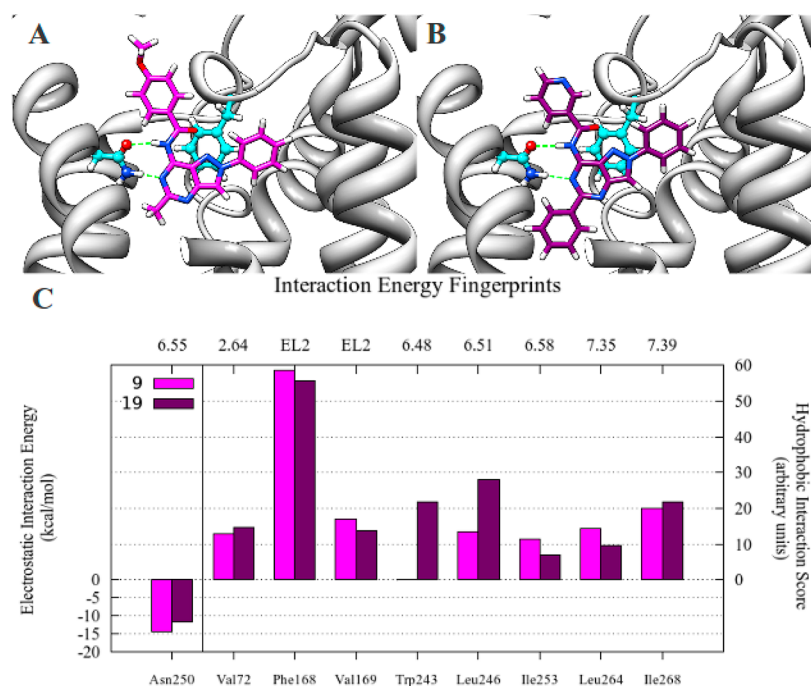


Figure 2. Most energetically favored docking poses obtained for compound **9** (A) and **19** (B) inside the hA₃ AR binding site. The poses are viewed from the membrane side facing TM6, TM7, and TM1. To aid visualization, the view of TM7 is partially omitted and hydrogen atoms are not displayed. Side chains of some amino acids important for ligand recognition and hydrogen bond interactions are highlighted. (C) Interaction energy fingerprints (IEFs) computed for the most energetically favored docking poses of compounds **9** and **19**: electrostatic interaction energy values and hydrophobic interaction scores are expressed in kcal/mol and arbitrary hydrophobic units, respectively.

among the herein reported compounds, i.e., derivative **9** ($K_i = 2.4$ nM).

Subsequently, the benzoyl moiety of derivatives **8** and **15** was replaced with the 2-furoyl (compounds **11** and **18**) and the 3- or 4-pyridoyl residues (derivatives **12**, **19** and **13**, **20**, respectively). These isosteric modifications were performed since in other classes of our previously reported AR antagonists^{22,23} maintained the capability of the molecules to properly interact with the hA₃ recognition site. The new derivatives **11–13** and **18** and **20** showed both nanomolar hA₃ affinity and high selectivity, similar to those of the parent compounds **8** and **15** and, more interestingly, the 7-(3-pyridylamido)-substituted derivative **19** had 6-fold higher hA₃ affinity than the parent **15**.

Also the presence of two acyl groups on the 7-amino substituent preserved high hA₃ AR affinity (compounds **28–30**), thus indicating the existence of a roomy receptor pocket able to hold the two bulky moieties. Introduction of the methoxy group as the R₂ substituent of the 7-acylamino derivatives **7–8**, **10**, **11** and **14**, **15**, **17** to give compounds **21–24** and **25–27**, respectively, did not produce a profitable effect. In fact, in only one case the hA₃ affinity was 3-fold enhanced (compound **21**), while in the others it was decreased (compounds **22**, **23**, **24**, **25**) or unchanged (compounds **26** and **27**). In contrast to the advantageous role of the acyl groups, a phenyl- or benzyl-carbamoyl moiety (compounds **31** and **32**, respectively) exerted a deleterious effect for the binding at the hA₃ receptor, as well as for the other receptor subtypes. Insertion of a para methoxy group on the 2-phenyl ring of the 7-ureido derivatives **31** and **32** did not enhance the AR affinity, being derivatives **33** and **34** as inactive as the parent derivatives **31** and **32**. The selected compounds **8**, **14**, **15**, **17**, **22**, **26–28** were tested to evaluate their antagonistic potencies to modulate

Cl-IB-MECA-inhibited cAMP accumulation in CHO cells expressing the hA₃ receptor. In accordance with the hA₃ AR affinity values, the IC₅₀ results (Table 1) showed that the tested compounds are hA₃ AR antagonists endowed with significant potencies.

Molecular Modeling Studies. With the aim of rationalizing the observed binding data, all the newly synthesized analogues were subjected to a molecular modeling investigation. We performed docking simulations at both the hA₃ AR model²⁵ and the crystallographic structure of hA_{2A} AR,²⁹ and we computed the *per-residue* electrostatic and hydrophobic contributions to the interaction energy for selected docking poses. The analysis of these contributions afforded IEFs: these interaction energy patterns highlight the key residues involved in the binding with the considered ligands, by providing a semiquantitative estimate of the occurring interactions and allowing a direct comparison of different ligands with respect to the quality of the ligand–receptor contacts.

The data reported in Table 1 reveal that the introduction of an amino moiety (**1–3**) in place of an oxo group (**A–C**) at the 7-position of the pyrazolo[4,3-*d*]pyrimidine scaffold causes a change of the affinity and selectivity profiles toward the different AR subtypes, by conferring to the new derivatives a good affinity for the A_{2A} AR. The most favorable docking poses obtained for compounds **1–3** at the A_{2A} AR help to explain the observed behavior. In Figure 1A, the corresponding hypothetical binding modes at the A_{2A} AR are depicted: the ligands (**1–3**) reside in the upper region of the transmembrane (TM) bundle and are anchored inside the binding cleft by a tight hydrogen bond network with the side chains of the highly conserved Asn253 (6.55)^{30,31} and Glu169 (EL2). The pyrazolo[4,3-*d*]pyrimidine (PP) core establishes an aromatic π – π stacking interaction with Phe168 (EL2) and hydrophobic

contacts with Trp246 (6.48) and Leu249 (6.51). The IEFs analysis (Figure 1B) identifies Asn253 (6.55) and Phe168 (EL2) as the residues mainly contributing to the interaction energy, with corresponding electrostatic energies and hydrophobic scores in the range 5–15 kcal/mol and 40–60 arbitrary units, respectively.

The loss of A_{2A} AR activity due to the introduction of an acyl moiety on the 7-amino group, to yield the corresponding 7-amido derivatives 7–30, can be ascribed to the loss of those key interactions. It is conceivable that the presence of a bulky substituent at this position forces the scaffold to adopt a different orientation into the binding cleft, by hampering the ligand to properly approach Asn253 (6.55) and Glu169 (EL2) and establish the above-described hydrogen bond network. On the contrary, the presence of sterically hindered substituents is well tolerated at the hA₃ AR. In this receptor subtype, the Glu169 residue is mutated to Val169: as a consequence, its binding pocket enables accommodation of bulky groups better than the other AR subtypes. Indeed, as indicated by the data in Table 1, the introduction of lipophilic and bulky substituents at the R₇ position (7–30) confers to the pyrazolo[4,3-*d*]pyrimidine scaffold a high degree of selectivity toward the hA₃ AR subtype.

To shed light on the molecular bases underlying this behavior, we report here the most favorable docking poses of two selected compounds, **9** and **19**, which represent two among the most active derivatives of the methyl- (R₅ = CH₃) and phenyl- (R₅ = Ph) substituted pyrazolopyrimidin-7-amino series, respectively.

In Figure 2A,B the hypothetical binding modes of **9** (K_i = 2.4 nM) and **19** (K_i = 3.2 nM), respectively, are depicted. The compounds share a common hypothetical binding mode: the ligand recognition occurs in the upper region of the TM bundle, the PP scaffold is surrounded by TMs 3, 5, 6, and 7 with the 2-phenyl ring and the R₅ groups pointing toward TM2 and TM6, respectively. The ligands are anchored inside the binding cleft by two stabilizing hydrogen bonds with the side chain of Asn250 (6.55) and an aromatic π - π stacking interaction with the side chain of Phe168 (EL2). As a result of this orientation, the R₇ substituent is directed outward from the binding cleft. The IEFs analysis for the two selected compounds (Figure 2C) reveals that further contributions to the whole interaction energy are afforded by hydrophobic contacts with other residues, namely, Val72 (2.64), Val169 (EL2), Leu246 (6.51), Ile253 (6.58), Leu264 (7.35), and Ile268 (7.39). At variance with derivative **9**, bearing a small alkyl group at the R₅ position, compound **19** also establishes a hydrophobic contact with Trp243 (6.48), an important residue in receptor activation and antagonist recognition.³¹ The placement of the ligands into the binding cleft also highlight that there is enough space to accommodate a para-methoxy moiety on the 2-phenyl ring.

From the docking analysis it is not easy to rationalize the observed low affinities of derivatives **31**–**34** bearing an urea moiety at the R₇ position. As it is generally recognized that the activity of disubstituted ureas strongly depends on their conformational state,³² we performed an *ab initio* study to identify the most stable conformer of the 7-ureido-pyrazolopyrimidine derivatives (see Supporting Information). From this analysis, it resulted that the most energetically favored species is the E,Z_b conformer (see Figure S1B) structure in which an intramolecular hydrogen bond leads to the formation of a six-membered pseudo cycle. We therefore ascribed the low affinity

showed by the 7-ureido-substituted derivatives to the adoption of such a conformation, that might remarkably change the orientation of the PP scaffold with respect to the binding modes predicted for the other derivatives (Figure 2A,B).

Finally, some of the most relevant ADME and physicochemical properties of all the new pyrazolopyrimidine derivatives were calculated (see Supporting Information, Table S1). The predicted data indicated that some properties, such as water solubility and blood–brain barrier penetration, could be ameliorated to improve the druggability profile of these derivatives.

Pharmacological Studies. Very recently it has been reported that A₃ AR modulation is relevant in chemotherapy-induced neuropathy.¹² On this basis, we tested some of the newly synthesized derivatives (**8**, **17**, **26**, **27**) by evaluating their effect on oxaliplatin-induced apoptosis in rat astrocyte cell cultures. It is well-known that astroglia cells play a key role in the central homeostasis, and therefore they would be expected to form an integral part of a response to CNS injury. Astrocytes activate several mechanisms that tend to decrease neuronal injury. In fact, they produce trophic factors, regulate transmitter and ion concentrations, thus having a direct influence on neuronal survival, synaptic transmission, and neural repair.³³ Hence, astrocytic functional impairments have the potential to induce neuronal dysfunction.³³ Moreover, astroglial cells have a pivotal role in neuropathy development.^{34,35}

The antineoplastic agent oxaliplatin is the standard treatment for advanced colorectal cancer; its limiting side effect is neurotoxicity that results in a neuropathic syndrome.^{36,37} In a primary cell culture of rat astrocytes, oxaliplatin was able to reduce cell viability (MTT assay, see Experimental Section) in a concentration-dependent manner showing LC50% > 100 μ M after 24 h incubation, and 16.0 \pm 0.1 μ M after 48 h. These values were in accordance with previous results indicating the strong resistance of astrocytes to noxious stimuli.^{38,39} Aimed at evaluating an early apoptotic effect we used 100 μ M oxaliplatin for 4 h incubation. This concentration was comparable to that used in an animal model of oxaliplatin-induced neuropathy (2.4 mg kg⁻¹, \sim 600 μ M)³⁷ and to that clinically used.⁴⁰

After 4 h incubation, 100 μ M oxaliplatin caused programmed cell death increasing caspase 3 activity up to 150%, with respect to the control condition fixed at 100% (Figure 3). All the tested pyrazolopyrimidines **8**, **17**, **26**, **27** were able to significantly prevent the oxaliplatin-dependent apoptosis when coincubated at micromolar concentration (10–0.1 μ M). Figure 3 shows the effect of compounds (1 μ M) on caspase 3 activity. Among them, compound **27** was the most effective in reducing the enzymatic activity. Subsequently, derivative **27** was tested on a human colon adenocarcinoma cell-line (HT-29) to assess whether it interferes with the oxaliplatin antineoplastic *in vitro* mechanism. The viability of HT-29 was measured in the presence of increasing concentration (0.1–100 μ M) of oxaliplatin, and its concentration-dependent lethal effect after 48 h incubation is described in Table 2. In the presence of **27** (10 μ M), oxaliplatin-dependent decrease of cell viability remained unaffected, suggesting a lack of interference with the anticancer activity. This evidence highlights a difference in oxaliplatin toxicity mechanism in normal nerve cells versus tumoral cells. Compound **27** selectively intervenes in neurotoxicity exerting protective effects on astrocytes.

In light of these interesting results, derivatives **8**, **17**, **26**, and **27** were tested for their ability to bind the rat A₃ AR. All the tested compounds displayed null rat A₃ receptor affinity,

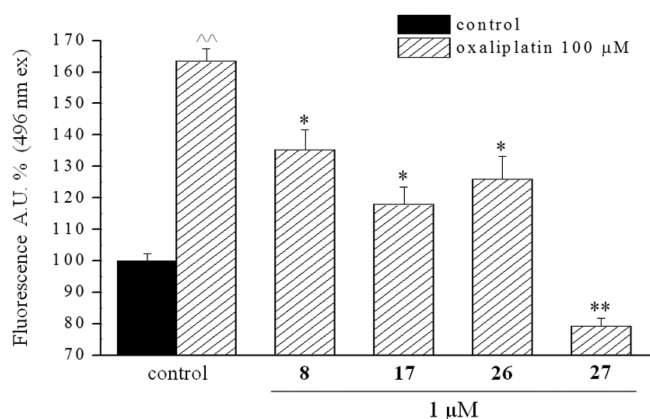


Figure 3. Antiapoptotic profile of derivatives **8**, **17**, **26**, **27**. Rat primary cortical astrocytes were exposed to 100 μM oxaliplatin for 4 h in the absence and in the presence of 1 μM of the tested compounds. Caspase 3 activity was evaluated by a fluorimetric assay. Values are expressed in percentage as mean \pm SEM. Control condition is fixed at 100%. $^{\wedge\wedge\wedge}P < 0.01$ with respect to control; $*P < 0.05$ and $**P < 0.01$ with respect to oxaliplatin.

notwithstanding their nanomolar affinity for the hA_3 receptor (Table 1). This result is in line with data obtained on most of the reported hA_3 antagonists, and it is due to the well-known species differences between human and rodent A_3 receptor.^{1,2} The null affinities for the rat A_3 AR of the tested compounds indicate that their protective effect on astrocytes should be ascribed to an A_3 receptor-independent mechanism.

In any case, these pyrazolopyrimidine derivatives still maintain high interest for their protective effect against oxaliplatin-induced toxicity in rat astrocytes.

CONCLUSION

The study reported here has led to the identification of a new series of potent and selective hA_3 AR antagonists, namely, the 2-arylpyrazolo[4,3-*d*]pyrimidin-7-amino derivatives. The presence of acyl moiety on the 7-amino group was found to be of paramount importance for both hA_3 AR affinity and selectivity. Indeed most of the 7-acylamino derivatives were potent and selective hA_3 AR antagonists. Molecular docking investigations performed at the hA_3 AR model permitted identification of the hypothetical binding mode of these new antagonists and to rationalize the observed SARs.

Some selected pyrazolo[4,3-*d*]pyrimidin-7-amides (**8**, **17**, **26**, **27**) proved to be effective in counteracting oxaliplatin-induced apoptosis, in rat astrocyte cell cultures, with a non- A_3 AR-dependent mechanism. Very interestingly, the most active compound **27** did not interfere with the antitumor activity of oxaliplatin on colon cancer HT-29 cell lines. Due to this intriguing pharmacological behavior, further investigations are in progress in our laboratory to develop new pyrazolo[4,3-

d]pyrimidines as protective agents against oxaliplatin-induced neurotoxicity.

EXPERIMENTAL SECTION

A. Chemistry. The microwave-assisted syntheses were performed using an Initiator EXP Microwave Biotage instrument (frequency of irradiation: 2.45 GHz). Silica gel plates (Merck F_{254}) and silica gel 60 (Merck, 70-230 mesh) were used for analytical and column chromatography, respectively. All melting points were determined on a Gallenkamp melting point apparatus. Elemental analyses were performed with a Flash E1112 Thermofinnigan elemental analyzer for C, H, N, and the results were within $\pm 0.4\%$ of the theoretical values. All final compounds revealed a purity not less than 95%. The IR spectra were recorded with a Perkin-Elmer Spectrum RX I spectrometer in Nujol mulls and are expressed in cm^{-1} . The ^1H NMR spectra were obtained with a Bruker Avance 400 MHz instrument. The chemical shifts are reported in δ (ppm) and are relative to the central peak of the solvent. The following abbreviations are used: s = singlet, d = doublet, t = triplet, m = multiplet, br = broad, and ar = aromatic protons.

General Procedure for the Synthesis of 1-Aryl-4-nitropyrazole-3-carboxamides 37²⁵ and 38. Compound **38** was prepared from the ester **36** in the same conditions previously described to prepare derivative **37** from **35**.²⁵ Briefly, a stream of ammonia was bubbled through a suspension of the ethyl pyrazole-3-carboxylates **35**–**36**²⁵ (3.0 mmol) in 33% aqueous ammonia solution (40 mL) for about 30 min. Then the suspension was stirred at room temperature for about 48 h (for **37**) or 24 h (for **38**). The solid was collected by filtration, washed with water, and recrystallized from 2-ethoxyethanol.

1-(4-Methoxyphenyl)-4-nitro-2-phenylpyrazole-3-carboxamide 38. Yield 75%; mp 232–233 $^{\circ}\text{C}$; ^1H NMR 3.83 (s, 3H, OMe), 7.13 (d, 2H, ar, $J = 9.4$ Hz), 7.85–7.88 (m, 3H, 2 ar + amide proton), 8.16 (br s, 1H, amide proton), 9.52 (s, 1H, H-5); Anal. Calc. for $\text{C}_{11}\text{H}_{10}\text{N}_4\text{O}_4$.

General Procedure for the Synthesis of 1-Aryl-4-nitropyrazole-3-carbonitriles 39–40. A suspension of **37** or **38** (2 mmol) in phosphorus oxychloride (5 mL) was microwave irradiated, respectively, at 160 $^{\circ}\text{C}$ for 30 min or 120 $^{\circ}\text{C}$ for 3 min. The excess of phosphorus oxychloride was distilled off and the residue was treated with water (about 5–10 mL). The obtained solid was collected by filtration and recrystallized.

4-Nitro-1-phenylpyrazole-3-carbonitrile 39. Yield 82%; mp 143–145 $^{\circ}\text{C}$ (cyclohexane/EtOH). ^1H NMR (DMSO- d_6) 7.54–7.63 (m, 3H, ar), 7.74–7.76 (m, 2H, ar), 8.72 (s, 1H, H-5); IR 2256. Anal. Calc. for $\text{C}_{10}\text{H}_6\text{N}_4\text{O}_2$.

1-(4-Methoxyphenyl)-4-nitropyrazole-3-carbonitrile 40. Yield 76%; mp 152–154 $^{\circ}\text{C}$ (EtOH). ^1H NMR (DMSO- d_6) 3.85 (s, 3H, OMe), 7.15 (d, 2H, ar, $J = 9.1$ Hz) 7.89 (d, 2H, ar, $J = 9.1$ Hz), 9.81 (s, 1H, H-5). IR 2251, 1538, 1342. Anal. Calc. for $\text{C}_{11}\text{H}_8\text{N}_4\text{O}_3$.

General Procedure for the Synthesis of 4-Amino-1-arylpyrazole-3-carbonitriles 41–42. A mixture of 4-nitropyrazoles **39**, **40** (2 mmol), cyclohexene (8 mmol), and 10% Pd/C (15% w/w with respect to the nitropyrazole) in EtOH (10 mL) was microwave irradiated at 150 $^{\circ}\text{C}$ for 15 min (compound **41**) or 10 min (compounds **42**). After being cooled at room temperature, the catalyst was filtered off and the solution was evaporated at reduced pressure to give a solid which was recrystallized from suitable solvent.

4-Amino-1-phenylpyrazole-3-carbonitrile 41. Yield 80%; mp 108–109 $^{\circ}\text{C}$ (H_2O). ^1H NMR (DMSO- d_6) 5.06 (br s, 2H, NH_2),

Table 2. Compound **27** Effect on Oxaliplatin-Affected HT-29 Cell Viability

oxaliplatin (μM)	HT-29 cell viability ^a						
	0	0.3	1	3	10	30	100
%	100.0	97.6 \pm 0.9	94.9 \pm 1.3	92.3 \pm 1.0	87.2 \pm 0.9	81.9 \pm 0.9	52.2 \pm 0.5
oxaliplatin + 27 (10 μM)		95.1 \pm 2.4	90.2 \pm 2.3	86.6 \pm 1.2	82.2 \pm 1.7	78.8 \pm 1.7	54.8 \pm 0.6

^aHT-29 cell viability was evaluated by MTT assay. HT-29 cells were treated with increasing oxaliplatin concentration (0.3–100 μM) in the presence or in the absence of **27** (10 μM) for 48 h. Values are expressed in percentage as mean \pm SEM. Control condition is fixed at 100%.

7.38 (t, 1H, ar, $J = 7.5$ Hz), 7.52 (t, 2H, ar, $J = 7.5$ Hz), 7.78 (s, 2H, ar, $J = 8.4$ Hz), 7.91 (s, 1H, H-5); IR 3377, 3340, 2331. Anal. Calc. for $C_{10}H_8N_4$.

4-Amino-1-(4-methoxyphenyl)pyrazole-3-carbonitrile 42. Yield 55%; mp 146–147 °C ($H_2O/EtOH$). 1H NMR ($DMSO-d_6$) 3.81 (s, 3H, OMe), 5.02 (br s, 2H, NH_2), 7.05 (d, 2H, ar, $J = 6.3$ Hz), 7.70 (d, 2H, ar, $J = 6.3$ Hz), 7.81 (s, 1H, H-5); IR 3343, 3338, 3330, 2218. Anal. Calc. for $C_{11}H_{10}N_4O$.

General Procedure for the Synthesis of 2-Arylpyrazolo[4,3-d]pyrimidin-7-amines 1–2, 4–5. A mixture of the 4-aminopyrazole-3-carbonitrile derivatives **41**, **42** (1 mmol), anhydrous ammonium acetate (2 mmol), and the suitable orthoester (1.5 mmol) was heated under microwave irradiation at 110 °C for 20 min (compound **1**), 130 °C for 30 min (compound **2**) or 10 min (compound **4**), and at 150 °C for 25 min (compound **5**). The mixture was cooled at room temperature and taken up with cyclohexane (3–5 mL). The resulting solid was collected, then suspended in 0.15 M $NaHCO_3$ solution (5–6 mL), and kept under stirring for 1–2 min. The crude product was collected by filtration, washed with water, and recrystallized.

5-Methyl-2-phenyl-2H-pyrazolo[4,3-d]pyrimidin-7-amine 1. Yield 80%; mp 295–297 °C (EtOAc). 1H NMR ($DMSO-d_6$) 3.38 (s, 3H, CH_3), 7.47 (t, 1H, ar, $J = 6.7$ Hz), 7.58–7.62 (m, 4H, 2ar + NH_2), 8.05 (d, 2H, ar, $J = 7.6$ Hz), 8.91 (s, 1H, H-3); IR 3471, 3445. Anal. Calc. for $C_{12}H_{11}N_5$.

2,5-Diphenyl-2H-pyrazolo[4,3-d]pyrimidin-7-amine 2. Yield 62%; mp 196–198 °C (cyclohexane/EtOAc). 1H NMR ($DMSO-d_6$) 7.42–7.52 (m, 4H, ar), 7.62–7.66 (m, 2H, ar), 7.81 (br s, 2H, NH_2), 8.10 (d, 2H, ar, $J = 7.7$ Hz), 8.41 (d, 2H, ar, $J = 8.0$ Hz), 9.13 (s, 1H, H-3); IR 3456, 3280, 1623. Anal. calc. for $C_{17}H_{13}N_5$.

2-(4-Methoxyphenyl)-5-methyl-2H-pyrazolo[4,3-d]pyrimidin-7-amine 4. Yield 72%; mp 269–270 °C (H_2O). 1H NMR ($DMSO-d_6$) 2.37 (s, 3H, Me), 3.84 (s, 3H, OMe), 7.14 (d, 2H, ar, $J = 9.1$ Hz), 7.61 (br s, 2H, NH_2), 7.95 (d, 2H, ar, $J = 9.1$ Hz), 8.80 (s, 1H, H-3). IR 3461, 3296, 1650. Anal. Calc. for $C_{13}H_{13}N_5O$.

2-(4-Methoxyphenyl)-5-phenyl-2H-pyrazolo[4,3-d]pyrimidin-7-amine 5. Yield 66%, mp 206–208 °C (EtOH). 1H NMR ($DMSO-d_6$) 3.86 (s, 3H, OMe), 7.17 (d, 2H, ar, $J = 9.0$ Hz), 7.43–7.46 (m, 3H, ar), 7.74 (br s, 2H, NH_2), 8.00 (d, 2H, ar, $J = 9.0$ Hz), 8.38 (d, 2H, ar, $J = 7.5$ Hz), 9.01 (s, 1H, H-3). IR 3465, 3296. Anal. Calc. for $C_{18}H_{15}N_5O$.

General Procedure for the Synthesis of 2-Aryl-5-benzylpyrazolo[4,3-d]pyrimidin-7-amines 3, 6. A mixture of the 4-aminopyrazole-3-carbonitrile derivatives **41**, **42** (1 mmol), anhydrous ammonium acetate (1.8 mmol), and ethyl phenyliminoacetate hydrochloride²⁸ (1.3 mmol) was heated under microwave irradiation at 150 °C for 15 min (compound **3**) or 10 min (compound **6**). The mixture, cooled at room temperature, was taken up with EtOAc (2–3 mL), and the solid which precipitated was filtered, washed with water (5–10 mL), and recrystallized.

5-Benzyl-2-phenyl-2H-pyrazolo[4,3-d]pyrimidin-7-amine 3. Yield 35%; mp 263–264 °C (EtOH). 1H NMR ($DMSO-d_6$) 3.96 (s, 2H, CH_2), 7.17 (s, 1H, ar, $J = 7.1$ Hz), 7.19–7.33 (m, 4H, ar), 7.48 (t, 1H, ar, $J = 7.1$ Hz), 7.59–7.64 (m, 4H, 2 ar + NH_2), 8.04 (d, 2H, ar, $J = 7.6$ Hz), 8.96 (s, 1H, H-3); IR 3438, 3315, 1661. Anal. Calc. for $C_{18}H_{15}N_5$.

5-Benzyl-2-(4-methoxyphenyl)-2H-pyrazolo[4,3-d]pyrimidin-7-amine 6. Yield 30%; mp 251–252 °C (2-ethoxyethanol). 1H NMR ($DMSO-d_6$) 3.84 (s, 3H, OMe), 3.95 (s, 2H, CH_2), 7.13–7.19 (m, 3H, ar), 7.25–7.31 (m, 4H, ar), 7.61 (br s, 2H, NH_2), 7.93 (d, 2H, ar, $J = 6.90$ Hz), 8.85 (s, 1H, H-3). IR: 3441, 3315. Anal. Calc. for $C_{19}H_{17}N_5O$.

General Procedure for the Synthesis of 7-Amido-substituted Pyrazolo[4,3-d]pyrimidine Derivatives 7, 9, 11, 14, 16–18, 21, 24–27. The title compounds were prepared by reacting the pyrazolopyrimidin-7-amino derivatives **1**, **2**, **4**, and **5** (1.3 mmol) with an excess of acetyl chloride (2.6 mmol), 4-methoxybenzoyl chloride (2 mmol), benzoyl chloride (2 mmol), 2-furoyl chloride (2.6 mmol), and phenylacetyl chloride (2.6 mmol) in anhydrous CH_2Cl_2 (15 mL) and pyridine (13 mmol). The mixture was stirred at room temperature for 2 h (compounds **14** and **17**) or 24 h (compounds **7** and **21**), or it was

heated at reflux for 5 h (compounds **11** and **26**), 24 h (compound **25**), 36 h (compounds **18** and **27**), 72 h (compounds **16** and **24**) or 6 days (compound **9**). The suspension was diluted with water (15 mL) and methylene chloride (15 mL). The organic phase was washed with water (15 mL \times 2) and anhydriified (Na_2SO_4). Evaporation of the solvent at reduced pressure afforded an oil which solidified upon treatment with diethyl ether (2–3 mL). All the crude derivatives were purified by recrystallization, except compounds **9**, **24**, and **26** which were chromatographed on silica gel column (eluent $CH_2Cl_2/EtOAc/MeOH$ 7:3:1, EtOAc/cyclohexane/MeOH 8:3:1, and $CH_2Cl_2/cyclohexane/CH_3CN$ 4.5:4.5:1, respectively) and then recrystallized.

7-Acetylamino-5-methyl-2-phenyl-2H-pyrazolo[4,3-d]pyrimidine 7. Yield 46%; mp 234–235 °C (EtOAc). 1H NMR ($DMSO-d_6$) 2.37 (s, 3H, Me), 2.59 (s, 3H, Me), 7.53 (t, 1H, ar, $J = 7.5$ Hz), 7.64 (t, 2H, ar, 7.5 Hz), 8.13 (d, 2H, ar, $J = 7.9$ Hz), 9.25 (s, 1H, H-3), 10.73 (s, 1H, NH). IR 3221, 3197, 1760. Anal. Calc. for $C_{14}H_{13}N_5O$.

5-Methyl-7-(4-methoxybenzoylamino)-2-phenyl-2H-pyrazolo[4,3-d]pyrimidine 9. Yield 25%; mp 227–228 °C (toluene). 1H NMR ($CDCl_3$) 2.62 (s, 3H, Me), 3.92 (s, 3H, OMe), 6.99 (d, 2H, ar, $J = 8.3$ Hz), 7.49 (t, 1H, ar, $J = 7.7$ Hz), 7.59 (t, 2H, ar, $J = 7.5$ Hz), 7.97 (d, 2H, ar, $J = 7.9$ Hz), 8.38 (s, 1H, H-3), 8.45 (d, 2H, ar, $J = 8.5$ Hz). IR 3399, 1643. Anal. Calc. for $C_{20}H_{17}N_5O_2$.

7-(2-Furoylamino)-5-methyl-2-phenyl-2H-pyrazolo[4,3-d]pyrimidine 11. Yield 35%; mp 229–231 °C (EtOH). 1H NMR ($CDCl_3$) 2.62 (s, 3H, Me), 6.60 (s, 1H, furane proton), 7.50 (t, 1H, ar, $J = 7.4$ Hz), 7.57–7.61 (m, 3H, 2 ar + furane proton), 7.67 (s, 1H, furane proton), 7.97 (d, 2H, ar, $J = 7.9$ Hz), 8.41 (br s, 1H, H-3), 14.22 (br s, 1H, exchangeable with D_2O). Anal. Calc. for $C_{17}H_{13}N_5O_2$.

7-Acetylamino-2,5-diphenyl-2H-pyrazolo[4,3-d]pyrimidine 14. Yield 62%; mp 228–230 °C (toluene). 1H NMR ($DMSO-d_6$) 2.51 (s, 3H, Me), 7.53 (m, 4H, ar), 7.67 (t, 2H, ar, $J = 7.8$ Hz), 8.18 (d, 2H, ar, $J = 7.8$ Hz), 8.45 (d, 2H, ar, $J = 8.0$ Hz), 9.46 (s, 1H, H-3), 10.88 (s, 1H, NH). IR 3246, 1676. Anal. Calc. for $C_{19}H_{13}N_5O$.

7-(4-Methoxybenzoylamino)-2,5-diphenyl-2H-pyrazolo[4,3-d]pyrimidine 16. Yield 78%; mp 233–235 °C (CH_3CN). 1H NMR ($DMSO-d_6$) 3.89 (s, 3H, OMe), 7.13 (d, 2H, ar, $J = 8.6$ Hz), 7.52–7.56 (m, 4H, ar), 7.65 (t, 2H, ar, $J = 7.8$ Hz), 8.09 (d, 2H, ar, $J = 8.6$ Hz), 8.14 (d, 2H, ar, $J = 8.2$ Hz), 8.43 (d, 2H, ar, $J = 5.8$ Hz), 9.50 (s, 1H, H-3), 11.23 (s, 1H, NH). Anal. Calc. for $C_{25}H_{19}N_5O_2$.

2,5-Diphenyl-7-phenylacetyl-2H-pyrazolo[4,3-d]pyrimidine 17. Yield 75%; mp 205–206 °C (toluene). 1H NMR ($DMSO-d_6$) 4.16 (s, 2H, CH_2), 7.28 (t, 1H, ar, $J = 7.1$ Hz), 7.38 (m, 4H, ar), 7.52 (m, 4H, ar), 7.68 (t, 2H, ar, $J = 7.6$ Hz), 8.18 (d, 2H, ar, $J = 8.4$ Hz), 8.45 (d, 2H, ar, $J = 7.9$ Hz), 9.47 (s, 1H, H-3), 11.18 (s, 1H, NH). IR 3485, 3385, 1709. Anal. Calc. for $C_{25}H_{19}N_5O$.

2,5-Diphenyl-7-(2-furoylamino)-2H-pyrazolo[4,3-d]pyrimidine 18. Yield 75%; mp 193–195 °C (EtOAc/cyclohexane). 1H NMR ($DMSO-d_6$) 6.79–6.81 (m, 1H, furane proton), 7.53–7.58 (m, 4H, ar), 7.64–7.69 (m, 3H, ar), 8.06 (s, 1H, furane proton), 8.16 (d, 2H, ar, $J = 7.7$ Hz), 8.47 (d, 2H, ar, $J = 8.1$ Hz), 9.52 (s, 1H, H-3), 11.14 (s, 1H, NH). Anal. Calc. for $C_{22}H_{15}N_5O_2$.

7-Acetylamino-2-(4-methoxyphenyl)-5-methyl-2H-pyrazolo[4,3-d]pyrimidine 21. Yield 46%; mp 189–190 °C (EtOAc). 1H NMR ($DMSO-d_6$) 2.36 (s, 3H, Me), 2.68 (s, 3H, Me), 3.68 (s, 3H, OMe), 7.17 (d, 2H, ar, $J = 9.0$ Hz), 8.04 (d, 2H, ar, $J = 9.0$ Hz), 9.14 (s, 1H, H-3), 10.69 (s, 1H, NH). IR 3336, 1709. Anal. Calc. for $C_{15}H_{15}N_5O_2$.

7-(2-Furoylamino)-5-methyl-2-(4-methoxyphenyl)-2H-pyrazolo[4,3-d]pyrimidine 24. Yield 25%; mp 221–223 °C (EtOH). 1H NMR ($CDCl_3$) 2.63 (br s, 3H, Me), 3.91 (s, 3H, OMe), 6.59 (br s, 1H, furane proton), 7.07 (d, 2H, ar, $J = 8.8$ Hz), 7.54 (br s, 1H, furane proton), 7.67 (s, 1H, furane proton), 7.87 (d, 2H, ar, $J = 8.8$ Hz), 8.31 (br s, 1H, H-3), 14.31 (br s, 1H, exchangeable with D_2O). Anal. Calc. for $C_{18}H_{15}N_5O_3$.

7-Acetylamino-2-(4-methoxyphenyl)-5-phenyl-2H-pyrazolo[4,3-d]pyrimidine 25. Yield 47%; mp 213–215 °C (cyclohexane/EtOAc). 1H NMR ($DMSO-d_6$) 2.50 (s, 3H, Me), 3.87 (s, 3H, OMe), 7.21 (d, 2H, ar, $J = 9.0$ Hz), 7.51–7.53 (m, 3H, ar), 8.09 (d, 2H, ar, $J = 9.0$ Hz), 8.44 (d, 2H, ar, $J = 7.4$ Hz), 9.34 (s, 1H, H-3), 10.82 (s, 1H, NH). IR 3224, 1700. Anal. Calc. for $C_{20}H_{17}N_5O_2$.

7-Benzoylamino-2-(4-methoxyphenyl)-5-phenyl-2H-pyrazolo[4,3-d]pyrimidine 26. Yield 40%; mp 205–207 °C (EtOH). 1H NMR

(DMSO- d_6) 3.86 (s, 3H, Me), 7.19 (d, 2H, ar, $J = 8.7$ Hz), 7.48–7.51 (m, 3H, ar), 7.59 (t, 2H, ar, $J = 7.3$ Hz), 7.67 (t, 1H, ar, $J = 7.0$ Hz), 8.06–8.07 (m, 4H, ar), 8.37–8.39 (m, 2H, ar), 9.41 (s, 1H, H-3), 11.38 (s, 1H, NH). IR 3259, 1662. Anal. Calc. for $C_{25}H_{19}N_5O_2$.

2-(4-Methoxyphenyl)-5-phenyl-7-phenylacetyl-amino-2H-pyrazolo[4,3-d]pyrimidine 27. Yield 25%; mp 168–170 °C (CH₃CN). ¹H NMR (DMSO- d_6) 3.87 (s, 3H, OMe), 4.15 (s, 2H, CH₂), 7.22 (d, 2H, ar, $J = 9.1$ Hz), 7.28 (t, 1H, ar, $J = 7.1$ Hz), 7.34–7.42 (m, 4H, ar), 7.49–7.51 (m, 3H, ar), 8.10 (d, 2H, ar, $J = 9.0$ Hz), 8.44 (d, 2H, ar, $J = 9.1$ Hz), 9.36 (s, 1H, H-3), 11.38 (s, 1H, NH). IR 3320, 1710. Anal. Calc. for $C_{26}H_{21}N_5O_2$.

General Procedure for the Synthesis of 7-Amido-substituted Pyrazolo[4,3-d]pyrimidine Derivatives 8, 10, 12, 13, 15, 19, 20, 22, 23. A mixture of the pyrazolopyrimidin-7-amino derivatives **1**, **2**, **4** (1 mmol), the suitable carboxylic acid (6 mmol), 1-(3-(dimethylamino)propyl)-3-ethyl-carbodiimide hydrochloride (6 mmol), 1-hydroxybenzotriazole hydrochloride (6 mmol), triethylamine (15 mmol), and 4-(dimethylamino)pyridine (0.1 mmol) in anhydrous dimethylformamide (2–3 mL) was stirred at room temperature for about 4 h (compound **22**), 7 h (compound **8**), 72 h (compounds **12**, **15**, **19** and **20**), and one week (compounds **10** and **23**). The suspension was diluted with water (about 15–20 mL), and the resulting solid was collected by filtration (compounds **8**, **15**, **19**, and **20**) or extracted with CH₂Cl₂ (15 mL × 3) (compounds **10**, **12**, **13**, **22**, and **23**). The combined organic extracts were anhydridified (Na₂SO₄), and the solvent was evaporated at reduced pressure. Derivatives **12**, **13**, **15**, **19**, **20**, **22**, and **23** were recrystallized, while compounds **8** and **10** were purified by column chromatography (eluent cyclohexane/EtOAc/MeOH 2:3:1 and EtOAc, respectively) and then recrystallized.

7-Benzoylamino-5-methyl-2-phenyl-2H-pyrazolo[4,3-d]pyrimidine 8. Yield 35%; mp 222–223 °C (EtOAc). ¹H NMR (CDCl₃) 2.72 (s, 3H, Me), 7.46–7.59 (m, 6H, ar), 7.95 (d, 2H, ar, $J = 7.7$ Hz), 8.38–8.39 (m, 2H, ar), 8.44 (s, 1H, H-3). IR 3156, 1621. Anal. Calc. for $C_{19}H_{15}N_5O$.

5-Methyl-2-phenyl-7-phenylacetyl-amino-2H-pyrazolo[4,3-d]pyrimidine 10. Yield 20%; mp 193–194 °C (MeOH). ¹H NMR (DMSO- d_6) 2.59 (s, 3H, Me), 4.04 (s, 2H, CH₂), 7.27 (t, 1H, ar, $J = 7.2$ Hz), 7.35–7.40 (m, 4H, ar), 7.53 (t, 1H, ar, $J = 7.4$ Hz), 7.64 (t, 2H, ar, $J = 7.7$ Hz), 8.12 (d, 2H, ar, $J = 7.8$ Hz), 9.26 (s, 1H, H-3), 10.98 (br s, 1H, NH). Anal. Calc. for $C_{20}H_{17}N_5O$.

5-Methyl-2-phenyl-7-(3-pyridoylamino)-2H-pyrazolo[4,3-d]pyrimidine 12. Yield 65%; mp 217–219 °C (EtOAc). ¹H NMR (CDCl₃) 2.67 (s, 3H, Me), 7.44–7.53 (m, 2H, 1 ar + pyridine proton), 7.60 (t, 2H, ar, $J = 7.4$ Hz), 7.98 (d, 2H, ar, $J = 8.5$ Hz), 8.44 (s, 1H, pyridine H-2 proton), 8.72–8.79 (m, 2H, pyridine protons), 9.64 (s, 1H, H-3), 14.57 (br s, 1H, exchangeable with D₂O). IR 3368, 1622. Anal. Calc. for $C_{18}H_{14}N_6O$.

5-Methyl-2-phenyl-7-(4-pyridoylamino)-2H-pyrazolo[4,3-d]pyrimidine 13. Yield 55%; mp 200–201 °C (EtOH). ¹H NMR (DMSO- d_6) 2.56 (s, 3H, Me), 7.49 (t, 1H, ar, $J = 7.3$ Hz), 7.60 (t, 2H, ar, $J = 7.6$ Hz), 7.99–8.03 (m, 4H, 2 ar + 2 pyridine protons), 8.80 (d, 2H, pyridine protons, $J = 5.8$ Hz), 9.18 (br s, 1H, H-3). Anal. Calc. for $C_{18}H_{14}N_6O$.

7-Benzoylamino-2,5-diphenyl-2H-pyrazolo[4,3-d]pyrimidine 15. Yield 40%; mp 248–249 °C (tetrahydrofuran/H₂O). ¹H NMR (DMSO- d_6) 7.51–7.71 (m, 9 H, ar), 8.08 (d, 2H, ar, $J = 7.5$ Hz), 8.15 (d, 2H, ar, $J = 7.6$ Hz), 8.40–8.41 (m, 2H, ar), 9.42 (s, 1H, H-3), 11.45 (br s, 1H, NH). IR 3243, 1676. Anal. Calc. for $C_{24}H_{17}N_5O$.

2,5-Diphenyl-7-(3-pyridoylamino)-2H-pyrazolo[4,3-d]pyrimidine 19. Yield 75%; mp 227–229 °C (EtOH). ¹H NMR (DMSO- d_6) 7.51–7.68 (m, 7H, 6 ar + pyridine proton), 8.16 (d, 2H, ar, $J = 7.9$ Hz), 8.35–8.37 (m, 3H, 2 ar + pyridine proton), 8.88 (d, 1H, pyridine proton, $J = 4.6$ Hz), 9.18 (br s, 1H, pyridine proton), 9.52 (s, 1H, H-3), 11.70 (s, 1H, NH). Anal. Calc. for $C_{23}H_{16}N_6O$.

2,5-Diphenyl-7-(4-pyridoylamino)-2H-pyrazolo[4,3-d]pyrimidine 20. Yield 68%; mp 262–264 °C (EtOAc). ¹H NMR (DMSO- d_6) 7.50–7.66 (m, 6H, ar), 7.91–7.94 (d, 2H, pyridine protons, $J = 4.4$ Hz), 8.16 (d, 2H, ar, $J = 7.7$ Hz), 8.31–8.30 (m, 2H, ar), 8.83 (d, 2H, pyridine protons, $J = 4.4$ Hz), 9.54 (s, 1H, H-3), 11.77 (s, 1H, NH). Anal. Calc. for $C_{23}H_{16}N_6O$.

7-Benzoylamino-2-(4-Methoxyphenyl)-5-Methyl-2H-pyrazolo[4,3-d]pyrimidine 22. Yield 68%; mp 216–217 °C (EtOAc). ¹H NMR (DMSO- d_6) 2.50 (s, 3H, ar), 3.84 (s, 3H, OMe), 7.14 (d, 2H, ar, $J = 9.0$ Hz), 7.52–7.62 (m, 3H, ar), 7.93 (br s, 2H, ar), 8.14 (br s, 2H, ar), 9.01 (br s, 1H, H-3). Anal. Calc. for $C_{20}H_{17}N_5O_2$.

2-(4-Methoxyphenyl)-5-methyl-7-phenylacetyl-amino-2H-pyrazolo[4,3-d]pyrimidine 23. Yield 52%; mp 206–208 °C (EtOH). ¹H NMR (DMSO- d_6) 2.58 (s, 3H, Me), 3.86 (s, 3H, OMe), 4.02 (s, 2H, CH₂), 7.18 (d, 2H, ar, $J = 9.0$ Hz), 7.26 (t, 1H, ar, $J = 7.1$ Hz), 7.33–7.40 (m, 4H, ar), 8.04 (d, 2H, ar, $J = 8.9$ Hz), 9.17 (s, 1H, H-3), 10.99 (s, 1H, NH). IR 3204, 1686. Anal. Calc. for $C_{21}H_{19}N_5O_2$.

General Procedure for the Synthesis of 7-Diacylamino-substituted Pyrazolo[4,3-d]pyrimidine Derivatives 28–30. The title compounds were obtained by refluxing the 7-amino derivatives **1** or **2** (2 mmol) with an excess of benzoyl chloride (10 mmol) or 2-furoyl chloride (15 mmol) in anhydrous methylene chloride (5 mL) and pyridine (20 mmol). The suspension was stirred at room temperature for 4 h (compound **28**) or refluxed for 96 h (compounds **29** and **30**), then diluted with water (10 mL), and the resulting mixture was extracted with methylene chloride (15 mL × 3). The organic phase was anhydridified (Na₂SO₄) and evaporated at reduced pressure to yield a solid which was purified by column chromatography (compound **28**, eluent cyclohexane/EtOAc 7:3) or by recrystallization (compounds **29** and **30**).

7-Dibenzoylamino-2-phenyl-2H-pyrazolo[4,3-d]pyrimidine 28. Yield 20%; mp 249–250 °C. ¹H NMR (DMSO- d_6) 2.57 (s, 3H, Me), 7.37–7.41 (m, 4H, ar), 7.44–7.54 (m, 5H, ar), 7.85 (d, 2H, ar, $J = 7.9$ Hz), 7.90 (d, 4H, ar, $J = 7.3$ Hz), 8.58 (s, 1H, H-3). Anal. Calc. for $C_{26}H_{19}N_5O_2$.

5-Methyl-7-(difuro-2-ylamino)-2-phenyl-2H-pyrazolo[4,3-d]pyrimidine 29. Yield 35%; mp 231–233 °C (EtOH). ¹H NMR (DMSO- d_6) 2.55 (s, 3H, Me), 6.73–6.86 (m, 2H, furane protons), 7.45–7.46 (m, 2H, furane protons), 7.54 (t, 1H, ar, $J = 7.0$ Hz), 7.62 (t, 2H, ar, $J = 7.4$ Hz), 7.93 (s, 2H, furane protons), 7.98 (d, 2H, ar), 9.46 (s, 1H, H-3). IR 1702. Anal. Calc. for $C_{22}H_{15}N_5O_4$.

2,5-Diphenyl-7-(difuro-2-ylamino)-2H-pyrazolo[4,3-d]pyrimidine 30. Yield 15%; mp 269–271 °C (EtOAc/cyclohexane). ¹H NMR (CDCl₃) 6.53–6.55 (m, 2H, furane protons), 7.40–7.57 (m, 10H, 8 ar + 2 furane protons), 7.89 (d, 2H, ar, $J = 7.8$ Hz), 8.22–8.25 (m, 2H, furane protons), 8.72 (s, 1H, H-3). Anal. Calc. for $C_{27}H_{17}N_5O_4$.

General Procedure for the Synthesis of 7-Ureido-Substituted Pyrazolo[4,3-d]pyrimidine Derivatives 31–34. The suitable isocyanate (1.5 mmol) was added to a suspension of the 7-amino derivatives **1** or **4** (1 mmol) in anhydrous tetrahydrofuran (20 mL). The mixture was refluxed under nitrogen atmosphere until the disappearance of the starting material (about 1–2 h). The suspension was diluted with water (5–10 mL), and the resulting solid was collected, washed with diethyl ether and recrystallized. Compound **31** was purified by column chromatography (eluent EtOAc).

5-Methyl-2-phenyl-7-(3-phenylureido)-2H-pyrazolo[4,3-d]pyrimidine 31. Yield 30%; mp 240–242 °C. ¹H NMR (CDCl₃) 2.80 (s, 3H, Me), 7.17 (t, 1H, ar, $J = 7.3$ Hz), 7.41 (t, 2H, ar, $J = 7.7$ Hz), 7.50–7.54 (m, 1H, ar), 7.61 (t, 2H, ar, $J = 7.6$ Hz), 7.67 (d, 2H, ar, $J = 7.9$ Hz), 7.90 (d, 2H, ar, $J = 7.9$ Hz), 8.15 (br s, 1H, NH), 8.48 (s, 1H, H-3), 12.10 (br s, 1H, NH). Anal. Calc. for $C_{19}H_{15}N_6O_2$.

7-(3-Benzylureido)-5-methyl-2-phenyl-2H-pyrazolo[4,3-d]pyrimidine 32. Yield 70%; mp 255–257 °C (toluene). ¹H NMR (CDCl₃) 2.67 (s, 3H, Me), 4.71 (d, 2H, CH₂, $J = 5.1$ Hz), 7.34–7.41 (m, 4H, ar), 7.51–7.58 (m, 4H, ar), 7.89 (d, 2H, ar, $J = 7.5$ Hz), 8.19 (br s, 1H, NH), 8.51 (s, 1H, H-3), 10.00 (br s, 1H, NH). Anal. Calc. for $C_{20}H_{18}N_6O$.

2-(4-Methoxyphenyl)-5-methyl-7-(3-phenylureido)-2H-pyrazolo[4,3-d]pyrimidine 33. Yield 65%; mp 241–243 °C (nitromethane). ¹H NMR (CDCl₃) 2.83 (s, 3H, Me), 3.93 (s, 3H, OMe), 7.09 (d, 2H, ar, $J = 8.0$ Hz), 7.17 (t, 1H, ar, $J = 7.2$ Hz), 7.41 (t, 2H, ar, $J = 7.3$ Hz), 7.66 (d, 2H, ar, $J = 8.0$ Hz), 7.82 (d, 2H, ar, $J = 7.5$ Hz), 8.24 (br s, 1H, NH), 8.45 (s, 1H, H-3), 12.00 (br s, 1H, NH). IR 3466, 1692. Anal. Calc. for $C_{20}H_{18}N_6O_2$.

7-(3-Benzylureido)-2-(4-methoxyphenyl)-5-methyl-2H-pyrazolo[4,3-d]pyrimidine 34. Yield 68%; mp 243–244 °C (EtOH/EtOAc). ¹H NMR (CDCl₃) 2.64 (s, 3H, Me), 3.93 (s, 3H, OMe), 4.70 (d, 2H,

CH₂, $J = 5.1$ Hz), 7.08 (d, 2H, ar, $J = 9.0$ Hz), 7.28–7.46 (m, 5H, ar), 7.78 (d, 2H, ar, $J = 8.56$ Hz), 8.20 (br s, 1H, NH), 8.43 (s, 1H, H-3), 10.02 (s, 1H, NH). IR 3376, 1694. Anal. Calc. for C₂₁H₂₀N₆O₂.

B. Computational Studies. All modeling studies were carried out on a 20 CPU (Intel Core2 Quad CPU 2.40 GHz) Linux cluster. Energy calculations and analyses of docking poses were performed with the Molecular Operating Environment (MOE, version 2010.10) suite.⁴¹

Three-Dimensional Structures of hA_{2A} AR and hA₃ AR. The crystallographic structure of hA_{2A} AR, in complex with the high affinity antagonist ZM241385 (PDB access code: 3EML),²⁹ and a previously proposed homology model of the hA₃AR²⁵ were used to perform molecular docking studies at these receptor subtypes.

The numbering of the amino acids follows the arbitrary scheme by Ballesteros and Weinstein: each amino acid identifier starts with the helix number, followed by the position relative to a reference residue among the most conserved amino acids in that helix, to which the number 50 is arbitrarily assigned.⁴²

Molecular Docking of hA₃ AR Antagonists. Ligand structures were built using the MOE-builder tool, as part of the MOE suite,⁴¹ and were subjected to a MMFF94x energy minimization until the rms conjugate gradient was <0.05 kcal mol⁻¹ Å⁻¹.

All antagonists were docked into the hypothetical TM binding site of the hA₃ AR model and the orthosteric binding site of the hA_{2A} AR crystal structure, by employing the docking tool of the GOLD suite.⁴³ For each compound, 25 independent docking runs were performed and searching was conducted within a user-specified docking sphere with the Genetic Algorithm protocol and the GoldScore scoring function.

Prediction of antagonist-receptor complex stability (in terms of corresponding pK_i value) and quantitative analysis for nonbonded intermolecular interactions (H-bonds, transition metal, water bridges, hydrophobic, electrostatic) were calculated and visualized using several tools implemented in the MOE suite.⁴¹ Electrostatic and hydrophobic contributions to the interaction energy of individual residues were calculated using MOE.⁴¹ To estimate the electrostatic contributions, atomic charges for the ligands were calculated with MOPAC⁴⁴ and the PM3/ESP methodology, whereas partial charges for the protein amino acids were computed with the AMBER99 force field.

Interaction Energy Fingerprints (IEFs). To analyze the ligand–receptor recognition mechanism in a more quantitative manner, we calculated the individual electrostatic and hydrophobic contributions to the interaction energy of each receptor residue involved in the binding with the ligand. In particular, the electrostatic contribution has been computed on the basis of the nonbonded electrostatic interaction energy term of the force field, whereas the hydrophobic contributions has been calculated by using the directional hydrophobic interaction term based on contact surfaces as implemented in the MOE scoring function.⁴¹ As a consequence, an energy (expressed in kcal/mol) is associated with the electrostatic contribution, whereas a score (the higher the better) is related to the hydrophobic contribution.

The analysis of these contributions have been reported as “interaction energy fingerprints” (IEFs), e.g., interaction energy patterns (graphically displayed as histograms) reporting the key residues involved in the binding with the considered ligands along with a quantitative estimate of the occurring interactions.

ADME and Physicochemical Properties. The predicted ADME and physicochemical properties have been calculated using StarDrop program.⁴⁵

C. Pharmacological Assays. Human Cloned A₁, A_{2A}, and A₃ AR Binding Assay. All synthesized compounds were tested to evaluate their affinity at human A₁, A_{2A}, and A₃ ARs. Displacement experiments of [³H]DPCPX (1 nM) to hA₁ CHO membranes (50 μg of protein/assay) and at least 6–8 different concentrations of antagonists for 120 min at 25 °C in 50 mM Tris HCl buffer pH 7.4 were performed.⁴⁶ Nonspecific binding was determined in the presence 1 μM of DPCPX (≤10% of the total binding). Binding of [³H]ZM-241385 (1 nM) to hA_{2A}CHO membranes (50 μg of protein/assay) was performed by using 50 mM Tris HCl buffer, 10 mM MgCl₂ pH 7.4 and at least 6–8 different concentrations of antagonists studied for an incubation time

of 60 min at 4 °C.⁴⁷ Nonspecific binding was determined in the presence of 1 μM ZM-241385 and was about 20% of total binding. Competition binding experiments to hA₃ CHO membranes (50 μg of protein/assay) were performed incubating 0.5 nM [¹²⁵I]AB-MECA, 50 mM Tris HCl buffer, 10 mM MgCl₂, 1 mM EDTA, pH 7.4, and at least 6–8 different concentrations of examined ligands for 60 min at 37 °C.⁴⁸ Nonspecific binding was defined as binding in the presence of 1 μM AB-MECA and was about 20% of total binding. Bound and free radioactivity were separated by filtering the assay mixture through Whatman GF/B glass fiber filters by using a Brandel cell harvester. The filter bound radioactivity was counted by Scintillation Counter Packard Tri Carb 2810 TR with an efficiency of 58%.

Rat A₃ Receptor Binding Assay. Selected compounds were tested for evaluating their affinity at rat A₃ adenosine receptors expressed in HEK293 cells (Perkin-Elmer, Boston, USA). Competition binding experiments to rA₃ HEK membranes (10 μg of protein/assay) were performed incubating 0.5 nM [¹²⁵I]AB-MECA, 50 mM Tris–HCl buffer, 10 mM MgCl₂, 1 mM EDTA, pH 7.4, and at least 6–8 different concentrations of examined ligands for 60 min at 37 °C.⁴⁹ Nonspecific binding was defined as binding in the presence of 1 μM AB-MECA and was about 20% of total binding. Bound and free radioactivity were separated by filtering the assay mixture through Whatman GF/B glass fiber filters by using a Brandel cell harvester. The filter bound radioactivity was counted by Scintillation Counter Packard Tri Carb 2810 TR with an efficiency of 58%.

Measurement of Cyclic AMP Levels in CHO Cells Transfected with hA_{2B} or hA₃ ARs. CHO cells transfected with hAR subtypes were washed with phosphate-buffered saline, diluted trypsin and centrifuged for 10 min at 200g. The cells (1 × 10⁶ cells/assay) were suspended in 0.5 mL of incubation mixture (mM): NaCl 15, KCl 0.27, NaH₂PO₄ 0.037, MgSO₄ 0.1, CaCl₂ 0.1, Hepes 0.01, MgCl₂ 1, glucose 0.5, pH 7.4 at 37 °C, 2 IU/mL adenosine deaminase, and 4-(3-butoxy-4-methoxybenzyl)-2-imidazolidinone (Ro 20-1724) as phosphodiesterase inhibitor and preincubated for 10 min in a shaking bath at 37 °C. The potency of antagonists to the A_{2B} AR was determined by the inhibition of NECA (200 nM)-induced cyclic AMP production. In addition, the potency of antagonists to the A₃ ARs was determined in the presence of forskolin 1 μM and Cl-IB-MECA (100 nM) that mediated inhibition of cyclic AMP levels. The reaction was terminated by the addition of cold 6% trichloroacetic acid (TCA). The TCA suspension was centrifuged at 2000g for 10 min at 4 °C, and the supernatant was extracted four times with water saturated diethyl ether. The final aqueous solution was tested for cyclic AMP levels by a competition protein binding assay. Samples of cyclic AMP standard (0–10 pmol) were added to each test tube containing [³H] cyclic AMP and incubation buffer (trizma base 0.1 M, aminophylline 8.0 mM, 2-mercaptoethanol 6.0 mM, pH 7.4). The binding protein prepared from beef adrenals was added to the samples previously incubated at 4 °C for 150 min, and, after the addition of charcoal, was centrifuged at 2000g for 10 min. The clear supernatant was counted in a Scintillation Counter Packard Tri Carb 2810 TR with an efficiency of 58%.⁴⁹

Data Analysis. The protein concentration was determined according to a Bio-Rad method⁵⁰ with bovine albumin as a standard reference. Inhibitory binding constant (K_i) values were calculated from those of IC₅₀ according to Cheng & Prusoff equation $K_i = IC_{50}/(1 + [C^*]/K_D^*)$, where [C*] is the concentration of the radioligand and K_D^{*} its dissociation constant.⁵¹ A weighted nonlinear least-squares curve fitting program LIGAND⁵² was used for computer analysis of inhibition experiments. IC₅₀ values obtained in cyclic AMP assay were calculated by nonlinear regression analysis using the equation for a sigmoid concentration–response curve (Graph-PAD Prism, San Diego, CA, U.S.A.).

Cell Cultures. Human colon cancer cell line HT-29 was obtained from American Type Culture Collection (Rockville, MD). HT-29 were cultured in Dulbecco's Modified Eagle's Medium (DMEM) high glucose with 20% fetal bovine serum (FBS). Media contained 2 mM L-glutamine, 1% essential aminoacid mix, 100 IU mL⁻¹ penicillin and 100 μg mL⁻¹ streptomycin (Sigma, Germany) in 5% CO₂ atmosphere at 37 °C.

Primary cultures of astrocytes were obtained according to the method described by McCarthy and De Vellis.⁵³ Briefly, the cerebral cortex of newborn (P1–P3) Sprague–Dawley rats (Harlan, Italy) were dissociated in Hank's balanced salt solution containing 0.5% trypsin/EDTA and 1% DNase (Sigma, Germany) for 30 min at 37 °C. Suspension was mechanically homogenized and filtered. Cells were plated in DMEM high glucose with 20% FBS. At confluency, primary glial cultures were used to isolate astrocytes removing microglia and oligodendrocytes by shaking. The purity of the astrocyte culture was determined by immunocytochemically staining for glial fibrillary acidic protein (GFAP) (Dako, Denmark). The cells were fixed in 4% paraformaldehyde, then incubated with the antibody (1:200) and visualized using Alexafluor conjugated secondary antibody. Of the cells in astrocyte cultures, 98% were positive for GFAP. Experiments were performed 21 days after cell isolation. Formal approval to conduct the experiments described was obtained from the Animal Subjects Review Board of the University of Florence. The ethical policy of the University of Florence complies with the Guide for the Care and Use of Laboratory Animals of the US National Institutes of Health (NIH Publication No. 85-23, revised 1996; University of Florence assurance number: A5278-01).

HT-29 and astrocytes were starved in serum-free DMEM overnight before all treatments.

Cells were incubated with 0.1–100 μ M oxaliplatin as described for each measurement (see below). The effects of tested compounds were evaluated allowing a concomitant incubation with oxaliplatin.

The duration time and concentration used in each set of experiments were chosen with respect to the method sensibility and specificity.

Caspase 3 Activity. Astrocytes were plated in 6-well plates (5 \times 10⁵/well) and grown in until 90% to 100% confluence. Cells were incubated with 100 μ M oxaliplatin for 4 h. After treatment cells were scraped in 100 μ M lysis buffer (200 mM Tris-HCl buffer, pH 7.5, containing 2 M NaCl, 20 mM EDTA, and 0.2% Triton X-100). Fifty microliters of the supernatants were incubated with 0.025 mM fluorogenic peptide caspase substrate rhodamine 110 bis-(N-CBZ-L-aspartyl-L-glutamyl-L-valyl-L-aspartic acid amide) (Z-DEVD-R110; Molecular Probes) at 25 °C for 30 min. The amount of cleaved substrate in each sample was measured in a 96-well plate fluorescent spectrometer (Perkin-Elmer; excitation at 496 nm and emission at 520 nm).

Cell Viability Assay. Cell viability was evaluated by the reduction of 3-(4,5-dimethylthiazol-2-yl)-2,5-diphenyltetrazolium bromide (MTT) as an index of mitochondrial compartment functionality. Cells were plated onto 96-well plates for cell culture (1 \times 10⁴ for astrocytes and 5 \times 10³ for HT-29), grown until confluence, and then treated for 24 or 48 h with different concentrations of oxaliplatin in DMEM. After extensive washing, 1 mg/mL MTT was added into each well and incubated for 2 h at 37 °C. After washing, the formazan crystals were dissolved in 100 μ L dimethyl sulfoxide. The absorbance was measured at 580 nm. Experiments were performed in quadruplicate on at least three different cell batches.

■ ASSOCIATED CONTENT

● Supporting Information

Conformational analysis data of the 7-ureido-pyrazolo[4,3-d]pyrimidine derivatives 31–34, ADME properties and combustion analysis data of the newly synthesized pyrazolopyrimidine derivatives. This material is available free of charge via the Internet at <http://pubs.acs.org>.

■ AUTHOR INFORMATION

Corresponding Author

*Tel +39 055 4573731 (V.C.); +39 049 8275704 (S.M.); fax +39 055 4573780 (V.C.); +39 049 8275366 (S.M.); e-mail: vittoria.colotta@unifi.it (V.C.); stefano.moro@unipd.it (S.M.).

Notes

The authors declare no competing financial interest.

■ ACKNOWLEDGMENTS

The synthetic work was supported by a grant of the Italian Ministry for University and Research (MIUR, FIRB RBNE03YA3L project). The molecular modeling work coordinated by S.M. was carried out with financial support from the University of Padova, Italy, and the Italian Ministry for University and Research (MIUR), Rome, Italy. S.M. is also very grateful to Chemical Computing Group for the scientific and technical partnership.

■ ABBREVIATIONS USED

AR, adenosine receptor; NECA, 5'-(N-ethyl-carboxamido)-adenosine; cAMP, cyclic adenosine monophosphate; Cl-IB-MECA, 2-chloro-N⁶-(3-iodobenzyl)5'-(N-methylcarboxamido)adenosine; DPCPX, 8-cyclopentyl-1,3-dipropyl-xanthine; ZM-241385, 4-(2-[7-amino-2-(2-furyl)[1,2,4]-triazolo[2,3-a][1,3,5]triazin-5-ylamino]ethyl)phenol; I-AB-MECA, N⁶-(4-amino-3-iodobenzyl)-5'-(N-methylcarboxamido)adenosine; CHO, chinese hamster ovary; IEFs, interaction energy fingerprints; TM, transmembrane; EL2, second extracellular loop; PP, pyrazolo[4,3-d]pyrimidine; RMSD, root-mean-square deviation; MOE, molecular operating environment; PES, potential energy surface; DMEM, Dulbecco's modified Eagle's medium; FBS, fetal bovine serum; GFAP, glial fibrillary acidic protein; MTT, 3-(4,5-dimethylthiazol-2-yl)-2,5-diphenyltetrazolium bromide

■ REFERENCES

- (1) Fredholm, B. B.; IJzerman, A. P.; Jacobson, K. A.; Klotz, K. N.; Linden, J. International union of Pharmacology XXV. Nomenclature and classification of adenosine receptors. *Pharmacol. Rev.* **2001**, *53*, 527–552.
- (2) Fredholm, B. B.; IJzerman, A. P.; Jacobson, K. A.; Linden, J.; Muller, C. E. International union of Pharmacology LXXXI. Nomenclature and classification of adenosine receptors. An up date. *Pharmacol. Rev.* **2011**, *63*, 1–34.
- (3) Jacobson, K. A.; Knutsen, L. J. S. P1 and P2 purine and pyrimidine receptor ligands. In *Purinergic and Pyrimidineric Signalling*; Abbracchio, M. P., Williams, M., Eds; Springer: Berlin, 2001; Handbook of Experimental Pharmacology, Vol. 151/1, pp 129–175.
- (4) Borea, P. A.; Gessi, S.; Bar-Yehuda, S.; Fishman, P. A₃ adenosine receptor: pharmacology and role in disease. *Handb. Exp. Pharmacol.* **2009**, *193*, 297–327.
- (5) Shneyvays, V.; Leshem, D.; Zinman, T.; Mamedova, L. K.; Jacobson, K. A.; Shainberg, A. Role of adenosine A₁ and A₃ receptors in regulation of cardiomyocyte homeostasis after mitochondrial respiratory chain injury. *Am. J. Physiol. Heart Circ. Physiol.* **2005**, *288*, H279–H2801.
- (6) Schulte, G.; Fredholm, B. B. Signalling from adenosine receptors to mitogen-activated protein kinases. *Cell. Signal.* **2003**, *15*, 813–827.
- (7) Gessi, S.; Merighi, S.; Sacchetto, V.; Simioni, C.; Borea, P. A. Adenosine receptors and cancer. *Biochim. Biophys. Acta* **2011**, *1808*, 1400–1412.
- (8) Brambilla, R.; Cattabeni, F.; Ceruti, S.; Barbieri, D.; Franceschi, C.; Kim, Y.-C.; Jacobson, K. A.; Klotz, K.-N.; Lohse, M. J.; Abbracchio, M. P. Activation of the A₃ adenosine receptor affect cell cycle progression and cell growth. *Naunyn-Schmiedeberg's Arch. Pharmacol.* **2000**, *361*, 225–234.
- (9) Gessi, S.; Merighi, S.; Varani, K.; Leung, E.; Mac Lennan, S.; Borea, P. A. The A₃ adenosine receptor: an enigmatic player in cell biology. *Pharmacol. Ther.* **2008**, *117*, 123–140.
- (10) Boison, D.; Chen, J.-F.; Fredholm, B. B. Adenosine signaling and function in glial cells. *Cell Death Differ.* **2010**, *17*, 1071–1082.
- (11) Liu, W.; Tang, Y.; Feung, J. Cross talk between activation of microglia and astrocytes in pathological conditions in the central nervous system. *Life Sci.* **2011**, *89*, 141–146.

- (12) Chen, Z.; Janes, K.; Chen, C.; Doyle, T.; Bryant, L.; Tosh, D. K.; Jacobson, K. A.; Salvemini, D. Controlling murine and rat chronic pain through A₃ adenosine receptor activation. *FASEB J.* **2012**, *26*, 1855–1865.
- (13) Pedata, F.; Pugliese, A. M.; Coppi, E.; Popoli, P.; Morelli, M.; Schwarzschild, M. A.; Melani, A. Adenosine in the central nervous system: effects on neurotransmission and neuroprotection. *Immun., Endoc. Metab. Agents Med. Chem.* **2007**, *7*, 304–321.
- (14) Taliani, S.; Bellandi, M.; La Motta, C.; Da Settimo, F. A₃ receptor ligands: past, present and future trends. *Curr. Top. Med. Chem.* **2010**, *10*, 942–975.
- (15) Colotta, V.; Catarzi, D.; Varano, F.; Cecchi, L.; Filacchioni, G.; Martini, C.; Trincavelli, L.; Lucacchini, A. 1,2,4-Triazolo[4,3-a]quinoxalin-1-one: a versatile tool for the synthesis of potent and selective adenosine receptor antagonists. *J. Med. Chem.* **2000**, *43*, 1158–1164.
- (16) Colotta, V.; Catarzi, D.; Varano, F.; Cecchi, L.; Filacchioni, G.; Martini, C.; Trincavelli, L.; Lucacchini, A. Synthesis and structure-activity relationships of a new sets of 2-arylpyrazolo[3,4-c]quinoline derivatives as adenosine receptor antagonists. *J. Med. Chem.* **2000**, *43*, 3118–3124.
- (17) Colotta, V.; Catarzi, D.; Varano, F.; Calabri, F. R.; Lenzi, O.; Filacchioni, G.; Trincavelli, L.; Martini, C.; Deflorian, F.; Moro, S. 1,2,4-Triazolo[4,3-a]quinoxalin-1-one moiety as an attractive scaffold to develop new potent and selective human A₃ adenosine receptor antagonists: synthesis, pharmacological and ligand-receptor modeling studies. *J. Med. Chem.* **2004**, *47*, 3580–3590.
- (18) Catarzi, D.; Colotta, V.; Varano, F.; Lenzi, O.; Filacchioni, G.; Trincavelli, L.; Martini, C.; Montopoli, C.; Moro, S. 1,2,4-Triazolo[1,5-a]quinoxaline as a versatile tool for the design of selective human A₃ adenosine receptor antagonists: synthesis, biological evaluation and molecular modeling studies of 2-(hetero)aryl- and 2-carboxy-substituted derivatives. *J. Med. Chem.* **2005**, *48*, 7932–7945.
- (19) Lenzi, O.; Colotta, V.; Catarzi, D.; Varano, F.; Filacchioni, G.; Martini, C.; Trincavelli, L.; Ciampi, O.; Marighetti, F.; Morizzo, E.; Moro, S. 4-Amido-2-aryl-1,2,4-triazolo[4,3-a]quinoxalin-1-ones as new potent and selective human A₃ adenosine receptor antagonists. Synthesis, pharmacological evaluation and ligand-receptor modeling studies. *J. Med. Chem.* **2006**, *49*, 3916–3925.
- (20) Colotta, V.; Catarzi, D.; Varano, F.; Capelli, F.; Lenzi, O.; Filacchioni, G.; Martini, C.; Trincavelli, L.; Ciampi, O.; Pugliese, A. M.; Pedata, F.; Schiesaro, A.; Morizzo, E.; Moro, S. New 2-arylpyrazolo[3,4-c]quinoline derivatives as potent and selective human A₃ adenosine receptor antagonists: synthesis, pharmacological evaluation, and ligand-receptor modeling studies. *J. Med. Chem.* **2007**, *50*, 4061–4074.
- (21) Morizzo, E.; Capelli, F.; Lenzi, O.; Catarzi, D.; Varano, F.; Filacchioni, G.; Vincenzi, F.; Varani, K.; Borea, P. A.; Colotta, V.; Moro, S. Scouting human A₃ adenosine receptor antagonist binding mode using a molecular simplification approach: from triazoloquinoxaline to a pyrimidine skeleton as a key study. *J. Med. Chem.* **2007**, *50*, 6596–6606.
- (22) Colotta, V.; Catarzi, D.; Varano, F.; Lenzi, O.; Filacchioni, G.; Martini, C.; Trincavelli, L.; Ciampi, O.; Traini, C.; Pugliese, A. M.; Pedata, F.; Morizzo, E.; Moro, S. Synthesis, ligand-receptor modeling studies and pharmacological evaluation of novel 4-modified-2-aryl-1,2,4-triazolo[4,3-a]quinoxalin-1-one derivatives as potent and selective human A₃ Adenosine Receptor Antagonists. *Bioorg. Med. Chem.* **2008**, *16*, 6086–6102.
- (23) Colotta, V.; Capelli, F.; Lenzi, O.; Catarzi, D.; Varano, F.; Poli, D.; Vincenzi, F.; Varani, K.; Borea, P. A.; Dal Ben, D.; Volpini, R.; Cristalli, G.; Filacchioni, G. Novel potent and highly selective human A₃ adenosine receptor antagonists belonging to the 4-amido-2-arylpyrazolo[3,4-c]quinoline series: molecular docking analysis and pharmacological studies. *Bioorg. Med. Chem.* **2009**, *17*, 401–410.
- (24) Colotta, V.; Lenzi, O.; Catarzi, D.; Varano, F.; Filacchioni, G.; Martini, C.; Trincavelli, L.; Ciampi, O.; Pugliese, A. M.; Traini, C.; Pedata, F.; Schiesaro, A.; Morizzo, E.; Moro, S. Pyrido[2,3-e]-1,2,4-triazolo[4,3-a]pyrazin-1-one as a new scaffold to develop potent and selective human A₃ adenosine receptor antagonists. Pharmacological evaluation, and ligand-receptor modeling studies. *J. Med. Chem.* **2009**, *52*, 2407–2419.
- (25) Lenzi, O.; Colotta, V.; Catarzi, D.; Varano, F.; Poli, D.; Filacchioni, G.; Varani, K.; Vincenzi, F.; Borea, P. A.; Paoletta, S.; Morizzo, E.; Moro, S. 2-Phenylpyrazolo[4,3-d]pyrimidin-7-one as a New Scaffold to obtain Potent and Selective Human A₃ Adenosine Receptor Antagonists: New Insights into the Receptor-Antagonist Recognition. *J. Med. Chem.* **2009**, *52*, 7640–7652.
- (26) Poli, D.; Catarzi, D.; Colotta, V.; Varano, F.; Filacchioni, G.; Daniele, S.; Trincavelli, L.; Martini, C.; Paoletta, S.; Moro, S. The Identification of the 2-Phenylphthalazin-1(2H)-one Scaffold as a New Decorable Core Skeleton for the Design of Potent and Selective Human A₃ Adenosine Receptor Antagonists. *J. Med. Chem.* **2011**, *54*, 2102–2113.
- (27) Lenzi, O.; Colotta, V.; Catarzi, D.; Varano, F.; Squarcialupi, L.; Filacchioni, G.; Varani, K.; Vincenzi, F.; Borea, P. A.; Dal Ben, D.; Lambertucci, C.; Cristalli, G. Synthesis, structure-affinity relationships and molecular modeling studies of novel pyrazolo[3,4-c]quinoline derivatives as adenosine receptor antagonists. *Bioorg. Med. Chem.* **2011**, *19*, 3757–3768.
- (28) McElvain, S. M.; Stevens, C. L. Ketene Acetals. XVI. Phenylketene Diethyl- and Dimethylacetals from the Pyrolysis of the Corresponding Orthoesters. *J. Am. Chem. Soc.* **1946**, *68*, 1917–1921.
- (29) Jaakola, V. P.; Griffith, M. T.; Hanson, M. A.; Cherezov, V.; Chien, E. Y. T.; Lane, J. R.; IJzerman, A. P.; Stevens, R. C. The 2.6 angstrom crystal structure of a human A_{2A} adenosine receptor bound to an antagonist. *Science* **2008**, *322*, 1211–1217.
- (30) Kim, J.; Wess, J.; van Rhee, M.; Schoneberg, T.; Jacobson, K. A. Site-directed mutagenesis identifies residues involved in ligand recognition in the human A_{2A} adenosine receptor. *J. Biol. Chem.* **1995**, *270*, 13987–13997.
- (31) Gao, Z.-G.; Chen, A.; Barak, D.; Kim, S.-K.; Muller, C. E.; Jacobson, K. A. Identification by site-directed mutagenesis of residues involved in ligand recognition and activation of the human A₃ adenosine receptor. *J. Biol. Chem.* **2002**, *277*, 19056–19063.
- (32) Galabov, A.; Galabov, B.; Neykova, N. Structure-Activity Relationship of Diphenylthiourea Antivirals. *J. Med. Chem.* **1980**, *23*, 1048.
- (33) Aschner, M.; Sonnewald, U.; Tan, K. H. Astrocyte modulation of neurotoxic injury. *Brain Pathol.* **2002**, *12*, 475–481.
- (34) Marchand, F.; Perretti, M.; McMahon, S. B. Role of the immune system in chronic pain. *Nat. Rev. Neurosci.* **2005**, *6*, 521–532.
- (35) Scholz, J.; Woolf, C. J. The neuropathic pain triad: neurons, immune cells and glia. *Nat. Neurosci.* **2007**, *10*, 1361–1368.
- (36) Gamelin, E.; Gamelin, L.; Bossi, L.; Quasthoff, S. Clinical aspects and molecular basis of oxaliplatin neurotoxicity: current management and development of preventive measures. *Semin. Oncol.* **2002**, *29*, 21–33.
- (37) Di Cesare Mannelli, L.; Zanardelli, M.; Failli, P.; Ghelardini, C. Oxaliplatin-induced neuropathy: oxidative stress as pathological mechanism. Protective effect of silibinin. *J. Pain* **2012**, *13*, 276–284.
- (38) Elekes, O.; Venema, K.; Postema, F.; Dringen, R.; Hamprecht, B.; Korf, J. Evidence that stress activates glial lactate formation in vivo assessed with rat hippocampus lactography. *Neurosci. Lett.* **1996**, *208*, 69–72.
- (39) Milligan, E. D.; Watkins, L. R. Pathological and protective roles of glia in chronic pain. *Nat. Rev. Neurosci.* **2009**, *10*, 23–36.
- (40) Cavaletti, G.; Tredici, G.; Petruccioli, M. G.; Dondè, E.; Tredici, P.; Marmiroli, P.; Minoia, C.; Ronchi, A.; Bayssas, M.; Erienne, G. G. Effects of different schedules of oxaliplatin treatment on the peripheral nervous system of the rat. *Eur. J. Cancer* **2001**, *37*, 2457–2463.
- (41) MOE (Molecular Operating Environment), version 2010.10; Chemical Computing Group Inc.: Montreal, Quebec, Canada, 2010.
- (42) Ballesteros, J. A.; Weinstein, H. Integrated methods for the construction of three dimensional models and computational probing of structure-function relationships in G-protein coupled receptors. *Methods Neurosci.* **1995**, *25*, 366–428.

- (43) *GOLD suite*, version 5.1; Cambridge Crystallographic Data Centre: Cambridge.
- (44) Stewart, J. J. P. *MOPAC 7*; Fujitsu Limited: Tokyo, Japan, 1993.
- (45) *StarDrop*, version 5.3; Optibrium Ltd: Cambridge, UK.
- (46) Borea, P. A.; Dalpiaz, A.; Varani, K.; Gessi, S.; Gilli, G. Binding thermodynamics at A_1 and A_{2A} adenosine receptors. *Life Sci.* **1996**, *59*, 1373–88.
- (47) Varani, K.; Rigamonti, D.; Sipione, S.; Camurri, A.; Borea, P. A.; Cattabeni, F.; Abbracchio, M. P.; Cattaneo, E. Aberrant amplification of A_{2A} receptor signalling in striatal cells expressing mutant huntingtin. *FASEB J.* **2001**, *5*, 1245–1247.
- (48) Varani, K.; Cacciari, B.; Baraldi, P. G.; Dionisotti, S.; Ongini, E.; Borea, P. A. Binding affinity of adenosine receptor agonists and antagonists at human cloned A_3 adenosine receptors. *Life Sci.* **1998**, *63*, 81–87.
- (49) Varani, K.; Gessi, S.; Merighi, S.; Vincenzi, F.; Cattabriga, E.; Benini, A.; Klotz, K.-N.; Baraldi, P. G.; Tabrizi, M.-A.; Mac Lennan, S.; Leung, E.; Borea, P. A. Pharmacological characterization of novel adenosine ligands in recombinant and native human A_{2B} receptors. *Biochem. Pharmacol.* **2005**, *70*, 1601–1612.
- (50) Bradford, M. M. A rapid and sensitive method for the quantification of microgram quantities of protein utilizing the principle of protein dye-binding. *Anal. Biochem.* **1976**, *72*, 248–254.
- (51) Cheng, Y. C.; Prusoff, W. H. Relationships between the inhibition constant (K_i) and the concentration of inhibitor which causes 50% inhibition (IC_{50}) of an enzymatic reaction. *Biochem. Pharmacol.* **1973**, *22*, 3099–3108.
- (52) Munson, P. J.; Rodbard, D. Ligand: a versatile computerized approach for the characterization of ligand binding systems. *Anal. Biochem.* **1980**, *107*, 220–239.
- (53) McCarthy, K. D.; de Vellis, J. Preparation of separate astroglial and oligodendroglial cell cultures from rat cerebral tissue. *J. Cell. Biol.* **1980**, *85*, 890–902.